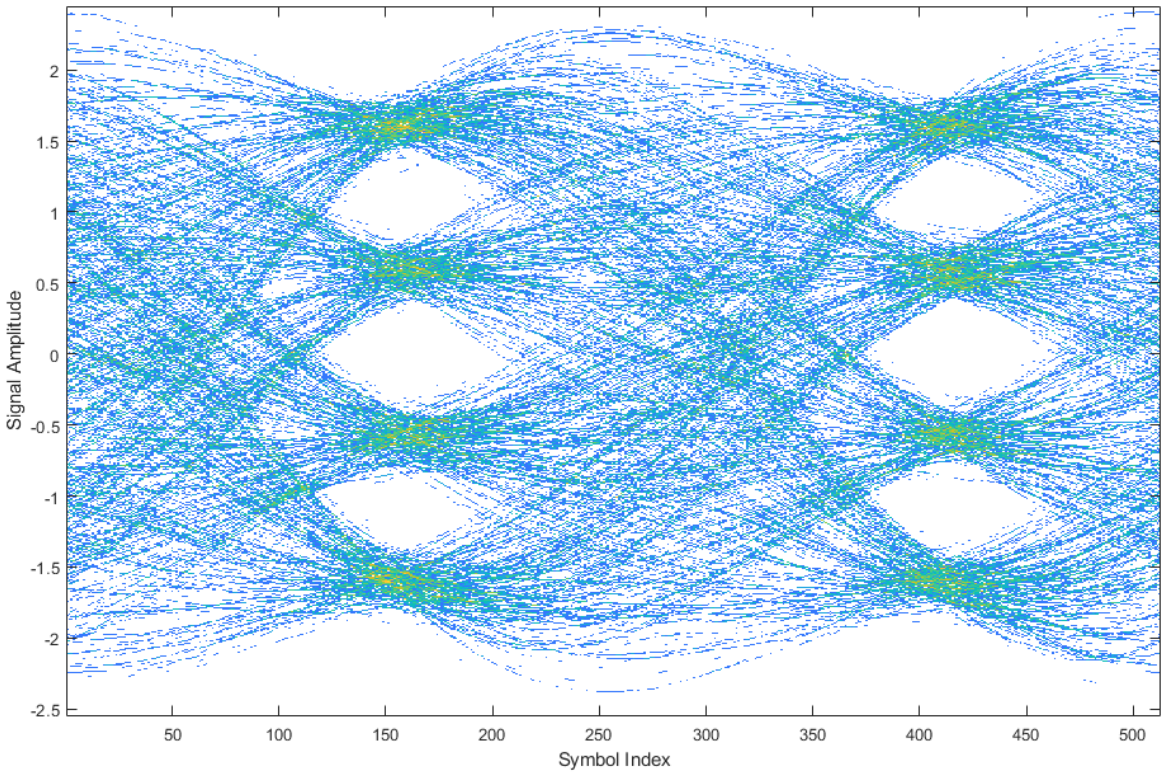

Mobile Optical Transmission Simulations

Development of a simulation framework in MATLAB

Master's thesis in Masters Programme of Information and Communication Technology

JACOPO PUCCINI

DEPARTMENT OF ELECTRICAL ENGINEERING
CHALMERS UNIVERSITY OF TECHNOLOGY
Gothenburg, Sweden 2025
www.chalmers.se

Master's thesis 2025

Mobile Optical Transmission Simulations

Development of a simulation framework in MATLAB

JACOPO PUCCINI

CHALMERS
UNIVERSITY OF TECHNOLOGY

Department of Electrical Engineering
Chalmers University of Technology
Gothenburg, Sweden 2025

Mobile Optical Transmission Simulations
Development of a simulation framework in MATLAB
JACOPO PUCCINI

Supervisor: Stefan Dahlfort, Standards & Technology, Business Unit Networks, Ericsson AB
Examiner: Tommy Svensson, Electrical Engineering

Master's thesis 2025
Department of Electrical Engineering
Chalmers University of Technology
SE-412 96 Gothenburg
Sweden
Telephone +46 31 772 1000

Cover: Eye diagram of a PAM-4 signal generated in MATLAB through Robochameleon´s simulation framework.

Typeset in LaTeX
Gothenburg, Sweden 2025

Mobile Optical Transmission Simulations
Development of a simulation framework in MATLAB
JACOPO PUCCINI
Department of Electrical Engineering
Chalmers University of Technology

Abstract

This thesis focuses on developing a robust simulation framework in MATLAB tailored for evaluating optical communication systems in mobile fronthaul networks. Leveraging the Robochameleon library, this research aims to model and analyze systems with high-speed optical links, addressing the increasing capacity demands of modern mobile networks (5G/6G). Critical developments include integrating a precise chirp compensation model to mitigate chromatic dispersion and a printed circuit board (PCB) simulation module for assessing signal degradation in electrical domains. The modular framework supports performance metrics like Bit Error Rate (BER) and Transmitter and Dispersion Eye Closure Quaternary (TDECQ) to validate system reliability. Results illustrate the effectiveness of chirp pre-compensation and signal equalizers in improving link performance while highlighting limitations in addressing severe impairments solely through linear compensations. Furthermore, the inclusion of additional models for signal processing components could significantly enhance the framework's accuracy and utility, facilitating broader adoption across diverse applications in next-generation optical network design and optimization.

Keywords: Optical Communications, Fronthaul, 5G, MATLAB, Simulation, Mobile Networks, Robochameleon, PAM4 Modulation, PCB.

Acknowledgements

Firstly, I want to thank Stefan for his support and guidance throughout the project and for showing me what a healthy work environment looks like, one that values young minds seeking their place after their studies. I also thank Tommy for setting up this thesis work and giving me this opportunity and Akshay for the helpful assistance in writing.
I dedicate this work to my family, who never stopped believing in my growth and my potential to become the person I am proud to be today. I also want to thank my beloved Denise, who never once stood in the way of me achieving this goal and showed me that only strong will and love can overcome distance. Un grazie di cuore a tutti.

Jacopo Puccini, Stockholm, June 2025

List of Acronyms

Below is the list of acronyms that have been used throughout this thesis listed in alphabetical order:

BER	Bit Error Rate
CW	Continuous Wave
DAC	Digital-to-Analog Converter
DFB	Distributed Feedback Laser
DFE	Decision Feedback Equalizer
DML	Directly Modulated Laser
DSP	Digital Signal Processing
DU	Distributed Unit
eCPRI	Enhanced Common Public Radio Interface
FFE	Feed-forward Equalizer
GVD	Group Velocity Dispersion
ISI	Inter-Symbol Interference
LPO	Linear Pluggable Optics
MIMO	Multiple Input-Multiple Output
MOPA	Mobile Optical Pluggables Alliance
NR	New Radio
NRZ	Non-Return-to-Zero
OMA	Optical Modulation Amplitude
PCB	Printed Circuit Board
PRBS	Pseudo-Random Binary Sequence
RAN	Radio Access Network
RIN	Relative Intensity Noise
RU	Radio Unit
SFPx	Small Form Factor (Pluggable)
SMF	Single-Mode Fiber
SNR	Signal-to-Noise Ratio
TDECQ	Transmitter and Dispersion Eye Closure Quaternary
TIA	Transimpedance Amplifier
WDM	Wavelength Division Multiplexing

Contents

List of Figures

Listings

1
Introduction

1.1 Background

Ericsson's mobile networks are deployed globally and mainly consist of baseband units (BBUs) and radio units (RUs). These units are interconnected by optical links, known as fronthaul links, which range from few tens of meters to 20 kilometers in length and support varying capacity requirements based on the deployment scenarios. With each new generation of mobile networks, such as the current 5G and the forthcoming 6G, the demand for capacity continues to increase, with current implementations requiring up to 50 Gbps per optical port and future systems targeting 100 to 200 Gbps, posing challenges to the fundamental limits of the optical and electrical components used in transmission. These advanced requirements [9] necessitate components that can operate within strict constraints, such as Small Form-factor Pluggable (SFP+) specifications, power consumption below 2.5W, and reliable operation across temperatures ranging from -40°C to +85°C. Consequently, Ericsson has recognized the importance of developing and utilizing simulations in computer environments to forecast the performance of these components and their capability to support the anticipated scalability of systems as capacity demands grow. The complexity of modern fronthaul systems requires comprehensive validation of both individual components and complete end-to-end link performance before physical implementation.

Currently, optics transmission simulations are mainly used in commercial products such as VPIphotonics that require expensive licenses. To explore lower cost alternatives, the company is interested in using Robochameleon, a MATLAB coding framework and component library designed for the simulation and experimental analysis of optical communication systems [1]. It was developed by the Digital Signal Processing (DSP) group at the Technical University of Denmark (DTU), along with multiple external collaborators. It aims to standardize methods and syntax for signal representation and function calls, which facilitates code sharing among researchers. The library includes physical models of components found in both coherent and incoherent optical communication systems, as well as standard DSP blocks that have been validated with real data. These capabilities extend to modeling various aspects of optical communications, from basic modulation formats to advanced signal processing algorithms, enabling accurate simulation of the complex interactions between optical and electrical domains present in modern fronthaul systems. The framework's open-source nature and validated component models provide Ericsson with the tools needed to address current technological challenges while preparing for

future advances in mobile network infrastructure, all while maintaining compliance with industry standards such as IEEE 802.3 and eCPRI specifications [2].

1.2 Aim

The thesis employs the Robochameleon library to model and evaluate fiber optical links for mobile fronthaul, adjusting parameters to closely mimic the current state of fibers connecting BBUs and RUs as researched by the industry [2]. The aim is to develop a simulation model that is as faithful as possible to real-world conditions, given the limitations of the existing scripts, and to generate data of practical relevance.

Additionally, this thesis aims to extend the framework by integrating modules capable of simulating the electrical channel of transmission components, such as printed circuit boards (PCBs) linking different components both at the transmitter and receiver. This recognizes that the transmission system extends beyond the optical Transmitter-Channel-Receiver paradigm.

1.3 Limitations

The use of models and simulations of real physical components that are subject to external environmental interactions (such as material degradation, site location, and human operation/interaction) has limitations in accurately representing real scenarios. As such, simulation results should be interpreted as comparative analyses between different engineering and design choices, rather than exact predictions of a real world optical link. Thus, these simulations need to be benchmarked with field or lab testing. The Robochameleon library was developed by multiple researchers, each applying their own assumptions based on individual biases and research goals. Despite these varying approaches, the scripts have been consistently corroborated, updated, and refined over time, making them reliable and robust models. Their validity has been verified multiple times, ensuring they are well-suited for accurate simulations. In the context of this thesis, the scenarios modeled rely on parameter choices that are thoroughly researched and referenced, providing coherence and reliability to the results obtained. Additionally, given the nature of this simulation system, some important elements such as power consumption and time delay are missing. This is due to the fact that power is treated as a feature or "object", in the programming language sense, of the signal propagating, but almost all units and modules do not account for their power consumptions. So, for instance, one cannot measure the energy prerequisites of some equalizer or how much energy is being dissipated by heat by some of the elements. The same goes for the time-related measurements, given that the speed of processing of the simulation is strictly dependent on the processing capability of the system running the MATLAB environment.

1.4 System Overview

In order to explain the design choices, an overview of a general mobile network deployed by Ericsson is presented.

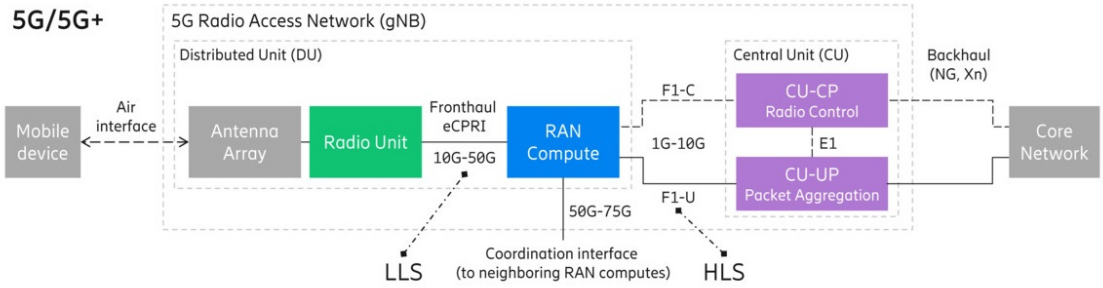

Figure 1.1: Overview of a 5G mobile network architecture [3]

The fronthaul section of the diagram illustrates the communication link between the radio unit (RU) and the distributed unit (DU), sometimes referred to as the Radio Access Network (RAN) Compute, utilizing high-speed, low-latency protocols such as the enhanced Common Public Radio Interface (eCPRI) for data transmission. The DU handles lower-layer RAN functions such as signal modulation, error correction, resource scheduling, and traffic management, ensuring real-time signal processing with minimal latency. This separation of RU and DU enables flexible deployments, centralized management, and resource pooling, enhancing scalability, and reducing costs. The fronthaul and DU architecture is critical for supporting advanced 5G features, including massive multiple input-multiple output (MIMO), beamforming, and low-latency applications. High-capacity fronthaul links are especially vital to handle the large data rates generated by these technologies, as they must efficiently transport traffic between the RU and the DU while meeting the low latency and reliability demands of real-time 5G use cases [4].

In our project, we are focusing on the connection between the RAN Compute and the RU, simulating various optical link configurations to evaluate their performance and quality in order to meet the stringent requirements for high-capacity and high-performance fronthaul links.

1.4.1 IEEE 802.3 Physical Layer Naming Convention

In order to quickly understand and reference the simulations of the standards, a general scheme for the naming of the physical layer (PHY) used in IEEE 802.3 protocols is presented:

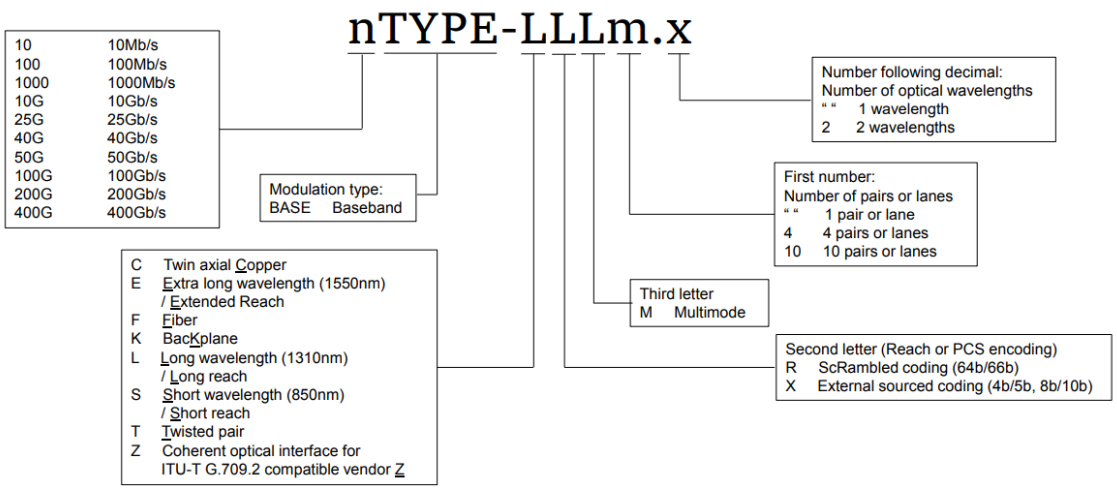

Figure 1.2: PHY naming scheme [5]

Given the scope of the project, we are only interested in a portion of these possible standards. For fronthaul optical links using the eCPRI protocol over single-mode fiber (SMF), several standardized high-speed optical interfaces are suitable for single-lane transmission. When focusing on single-mode fiber (SMF) implementations, the naming convention specifically identifies configurations using "1 pair or lane" through the absence of a number (m) after the last letter. For fronthaul applications using the eCPRI protocol, the most relevant classifications are F (Fiber reach), S (Short reach), or L (Long reach), as these designate operation on high-speed optical links over SMF. The second letter in the format, either R or X, indicates the encoding method employed - whether scrambled coding (64b/66b) or external-sourced coding (4b/5b or 8b/10b) but these are dropped since we are testing raw performance with hard decoding. In single-wavelength transmission schemes operating on a single fiber, protocols such as 10GBASE-LR, 25GBASE-FR, or similar standards are particularly relevant due to their optimization for single-lane SMF links in fronthaul network architectures as well as 50GBASE-LR, which are of interest for higher capacities.

2
Theory

The following sections provide a structured overview of both the technological advances and simulation methodologies central to the study of modern mobile optical networks. We begin with a discussion of the growing demand and evolving requirements of mobile networks, followed by an quick look at fronthaul technology as a key enabler in next-generation architectures. Subsequently, we introduce the Robochameleon simulation framework used throughout this work, and detail the methodologies for evaluating system performance through script-based metrics.

2.1 Growing demand in mobile networks

The evolution of mobile networks demonstrates unprecedented growth in adoption and capacity requirements, with the adoption of 5G subscriptions showing remarkable momentum. As of the third quarter of 2024, global 5G subscriptions reached 2.1 billion, increasing by 163 million in just one quarter. Projections indicate close to 2.3 billion subscriptions by the end of 2024, accounting for more than 25 percent of all mobile subscriptions. This trajectory exceeds earlier predictions, with 5G now expected to become the dominant mobile access technology by subscription in 2027 [6]. This rapid expansion is driven by transformative applications such as autonomous driving, smart cities, and Industry 4.0, all of which rely on 5G's high-speed, low-latency capabilities to enable real-time connectivity and advanced automation. Compared to 4G, 5G delivers significantly enhanced network capacity, ultra-reliable low-latency communication (URLLC), and support for massive machine-type communications (mMTC), making it far better suited for these demanding scenarios [7, 8]. However, the journey toward universal mobile connectivity remains incomplete, with significant portions of the global population still lacking access to 5G technology, emphasizing the need to expand both coverage and capacity of mobile networks globally.

The scope of this evolution extends beyond mere subscription numbers and traffic volume. In densely populated urban areas, network densification, measured as traffic load per square kilometer, has become equally crucial as raw capacity. Analyst projections suggest that major metropolitan areas will need to handle 1-2 petabytes per square kilometer by 2025, driving parallel evolution in mobile transport network capacity and density. This escalation in requirements has elevated the importance of optical solutions in mobile networks, particularly evident in the changing economics of radio unit components, where the relative cost portion of optical components has

roughly doubled with 5G New Radio (NR) compared to previous generations [9].

In the realm of optical transport for mobile networks, a significant transformation is underway. Traditional approaches using simple 10G optical links are being rapidly superseded by demands for 25G, 50G, and even 100G connections. This evolution presents unique challenges in the optical domain, particularly when considering the industry's preference for smaller form factors and more efficient power consumption. Current optical components, especially pluggable transceivers designed primarily for data center applications, often fall short of modern mobile network requirements, driving initiatives like Mobile Optical Pluggables (MOPA) to develop industry specifications for optical components optimized specifically for mobile network deployment [10]. A critical challenge emerges in maintaining the popular SFPx form factor for increasingly complex optics as bit rates continue to increase. Some solutions to address these problems are direct fiber and short-reach, PAM-4 modulation, "coherent lite" solutions, and various wavelength division multiplexing schemes. Real-world measurements of 1.6 million fronthaul links show that 95% of the optical links operate below 2 km, highlighting the need for cost-effective single-mode short-distance optical transmitters. The evolution also brings unique environmental challenges. Mobile equipment must operate in demanding conditions, requiring optical components that function reliably at high temperatures (up to 85°C) with minimal heat dissipation mechanisms. Unlike data center equipment in controlled environments, mobile network components must maintain performance across wide temperature ranges while achieving a 15-year operational lifespan.

Looking ahead, timing precision becomes increasingly critical for 6G networks. While traditional applications tolerated tens of milliseconds of delay, emerging applications like haptic feedback and industrial robotics demand latencies below 1 ms. The transport layer faces its most challenging case in fronthaul applications, where latency must be contained to hundreds of microseconds while maintaining precise synchronization between radio units. The industry is also witnessing a trend toward "zero touch" automation and flexibility, requiring auto-negotiation and self-discovery capabilities at both endpoints of optical links. This evolution in mobile network architecture represents more than just increased bandwidth; it signals a fundamental shift in how networks are designed and operated. Success requires balancing demands for higher capacity and lower latency with practical constraints of power consumption, form factor, and cost-effectiveness, while ensuring the reliability and longevity expected of telecommunications infrastructure.

2.2 Fronthaul Technology in Modern Networks

Fronthaul plays a fundamental role in modern mobile networks, constituting critical point-to-point optical links that connect centralized signal processing locations to distributed radio units. As the industry has moved toward architectures such as Cloud-RAN and increasingly dense 5G deployments, fronthaul has become crucial for scaling performance, supporting flexibility, and enabling advanced radio features. With the exponential growth in site and traffic density, particularly in urban areas,

optimizing fronthaul is vital not just for capacity, but for maintaining coverage, spectrum efficiency, and operational simplicity [9]. The enhanced Common Public Radio Interface (eCPRI) protocol represents a key innovation for fronthaul, advancing beyond its predecessor by supporting lower bit rates via functional splits and flexible bandwidth allocation, which is essential for meeting explosive capacity growth in a cost-effective manner. eCPRI's flexibility directly addresses multi-vendor interoperability and cloud-native RAN requirements, and it helps reduce fronthaul traffic through smarter compression and packetization strategies. However, these advancements require corresponding progress in the underlying physical layer to handle the leap from traditional 10G optics to current 25G/50G deployments, and to future 100G and even 200G optical modules envisioned for 6G [11].
Bandwidth and latency constraints form a critical axis of fronthaul requirements, especially as forward-looking applications impose stringent limits: future industrial and immersive applications will drive requirements to sub-millisecond or even hundreds-of-microseconds fronthaul latency. This low-latency mandate is further complicated by the need for precise synchronization not just within a site, but across the network—in some cases, at nanosecond-scale accuracy between radios. Deployment scenarios are therefore highly diverse.

While most live fronthaul deployments exploit short, single-mode optical links, there is parallel demand for longer-reach and wavelength-multiplexed solutions in high-density urban environments. The industry is also pursuing more automated Operations & Maintenance (O&M) practices to match the sheer number of deployed links and keep operational complexity in check. In summary, fronthaul technology serves as the foundation for realizing high-performance, agile, and future-proof mobile networks. Innovations in protocols such as eCPRI, optical component design, and network automation are essential to meet the growing demands for bandwidth, latency, and resilience posed by 5G today and 6G in the near future. An effective fronthaul not only bridges the gap between centralized processing and distributed radios, but also defines the practical limits of next-generation wireless communication.

2.3 Robochameleon's working principle

The Robochameleon simulation framework is a MATLAB-based platform designed to simulate optical communication systems, offering a modular and class-based structure that ensures efficient simulation, reusability of components, and adherence to standardized development practices. At its core, the framework operates on a class-based design, where physical devices, algorithms, and modules are represented as reusable MATLAB classes. Signals, whether optical or electrical, are encapsulated as `signal_interface` objects, each storing parameters like power, frequency, and sampling rate. This architecture ensures both immutability and clarity in signal processing throughout the simulation flow.

A key concept in Robochameleon is the distinction between "units" and "modules." Units, such as **A**, **B**, **C**, and **D** in Figure 2.1, represent individual devices or funda-

mental functions (for example, lasers, modulators, or filters), effectively serving as the atomic building blocks of the simulation. Modules are higher-level constructs created by interconnecting multiple units and explicitly managing the flow of signals between them. For instance, in the illustrated module, inputs 1 and 2 are independently routed to units A and B, whose outputs are subsequently fed into unit C. The outputs of unit C are then distributed, with one branch directed to unit D, and the outputs of D, alongside further outputs from C, collectively forming the multi-output interface of the overall module. By clearly mapping these input and output connections, such as output 1 of A linking to input 1 of C, output 1 of B linking to input 2 of C, and so forth, the framework supports hierarchical and reusable model development. Moreover, a dedicated constants class (`const`) provides essential physical constants (e.g., the speed of light or Planck's constant), further enhancing the accuracy of simulations. This inter-unit connectivity is a direct outcome of Robochameleon's class-based paradigm, which facilitates both clear signal routing and modular reusability.

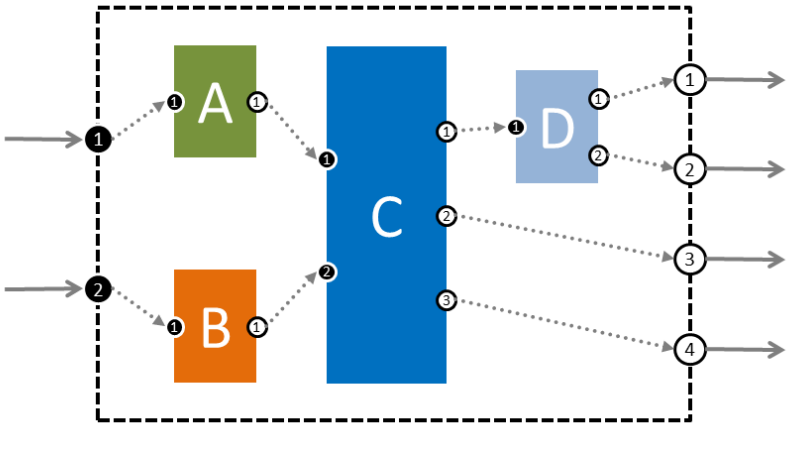

Figure 2.1: Block structure of modules and units in Robochameleon

Take SimpleIMTransmitter as an example (Figure 2.2): this module encapsulates the characteristics of an intensity-modulated (IM) transmitter. Within its design, it integrates the SimpleAWG_v1 module, responsible for arbitrary waveform generation, as a key component. The digital signal produced by the AWG is then branched to both an IntensityModulator_v1 (representing the IM device) and a Laser_v3 (providing the optical carrier). The laser output is also directed to the intensity modulator, where the modulation occurs. The setup is achieved by specifying the precise interconnections between these internal units and modules, ensuring that digital bit streams generated upstream are correctly processed, shaped, combined with the optical carrier, and finally output as analog optical signals ready for transmission. This modular approach offers significant advantages for signal processing inspection, analysis, and debugging. Since each module structure explicitly details how units are connected and signals are passed between them, users can systematically trace the life cycle of a signal through every stage of the simulation. The framework guarantees signal consistency by creating new `signal_interface` ob-

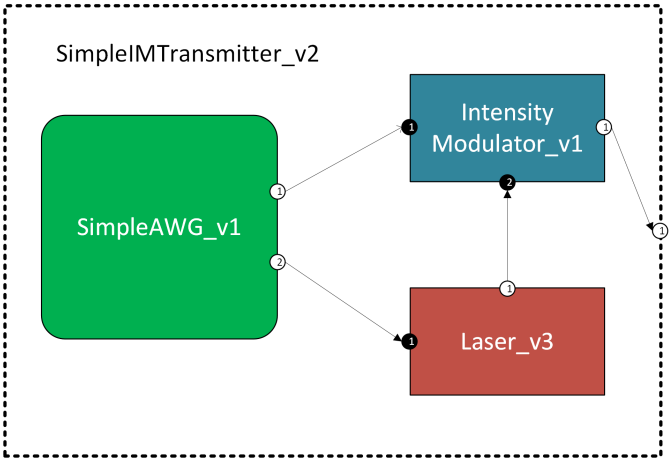

Figure 2.2: Intensity modulated transmitter

jects after each operation, thus allowing for clear checkpoints within the processing flow. During execution, state information is maintained within units and modules, and the framework facilitates reproducibility by allowing users to save and reload the internal state of every component. By representing optical communication systems in modular, hierarchical blocks, with clear interfaces and traceable signal flow, Robochameleon allows users to deeply analyze subsystem interactions, identify potential issues at each processing stage, and debug complex system behaviors. This structured and transparent approach underpins both the robustness and flexibility of Robochameleon as a simulation tool for current and next-generation optical system design.

2.4 Performance Metrics

In our project we are focused on the study and simulation of messages using Pulse Amplitude Modulation with 4 levels (PAM4), and for its analysis we can make use of different tools:

- **Bit Error Rate (BER) Analysis:** The BitErrorCounter_PAM_v1.m script provides a rigorous method for calculating the Bit Error Rate, a basic metric representing the ratio of incorrectly received bits to total transmitted bits. For PAM4 signals, which encode two bits per symbol across four distinct amplitude levels (Figure 2.3), BER analysis is particularly crucial. The reduced separation between levels makes the system more susceptible to errors stemming from noise and transmission impairments. The script implements symbol-to-bit mapping and demapping algorithms tailored for PAM4 encoding, ensuring precise error counting even in the presence of impairments such as jitter, inter-symbol interference (ISI), and various noise sources commonly observed in optical fronthaul links. Additionally, it provides a BER estimation derived from error vector magnitude (EVM) analysis, an effective approach for rapidly predicting error rates without requiring massive bit counts. This is particularly beneficial when simulating high-capacity fronthaul networks where memory or runtime limitations can occur. Given that fronthaul optical links typically operate close to system margins defined in standards like IEEE 802.3bs, accurately quantifying BER helps verify that system performance fulfills stringent requirements for error rates and transmission reliability.
- **Eye Diagram Visualization:** The PlotEyediagram_contour.m script generates colored eye diagrams that visually represent signal quality, an indispensable tool for physical layer analysis in optical fronthaul deployments. Unlike binary transmission's single eye, PAM4 signals exhibit three vertically stacked "eyes" (Figure 2.4), each corresponding to transitions between adjacent amplitude levels. In the context of fronthaul optical links, the eye diagram provides an immediate visual assessment of how signal integrity is influenced by the tight noise and jitter budgets specified in communication standards such as common public radio interface (CPRI), eCPRI, and IEEE 802.3. After each simulation run, generated waveforms are processed into eye diagrams, revealing the combined effects of noise, chromatic dispersion, component non-idealities, and ISI. Careful analysis of the vertical and horizontal openings delivers a direct measure of the signal-to-noise and timing margins available for reliable symbol detection, while transition steepness and zero crossing variation illuminate the presence of jitter and timing uncertainty, key concerns in high-density, low latency fronthaul scenarios. Comparing eye diagrams from different channel conditions helps engineers visually quantify the impact of network impairments and verify compliance with rigorous fronthaul link requirements.

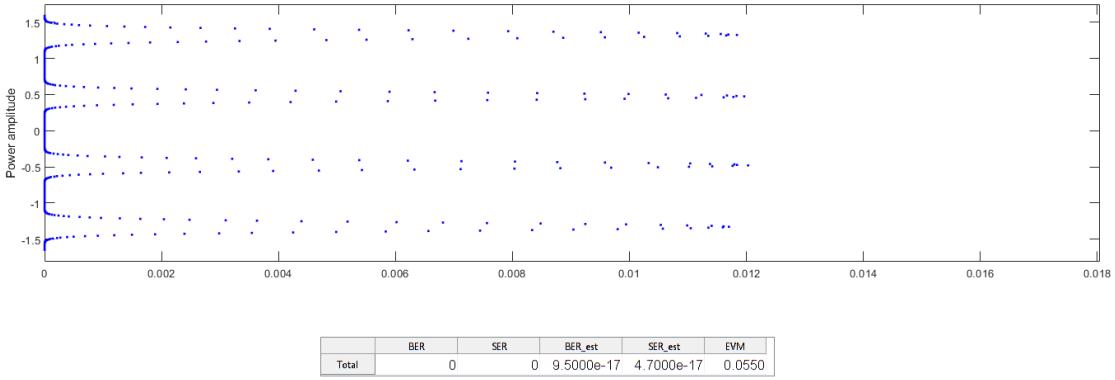

	BER	SER	BER_est	SER_est	EVM
Total	0	0	9.5000e-17	4.7000e-17	0.0550

Figure 2.3: Example of a received point distribution of PAM4 for BER calculation

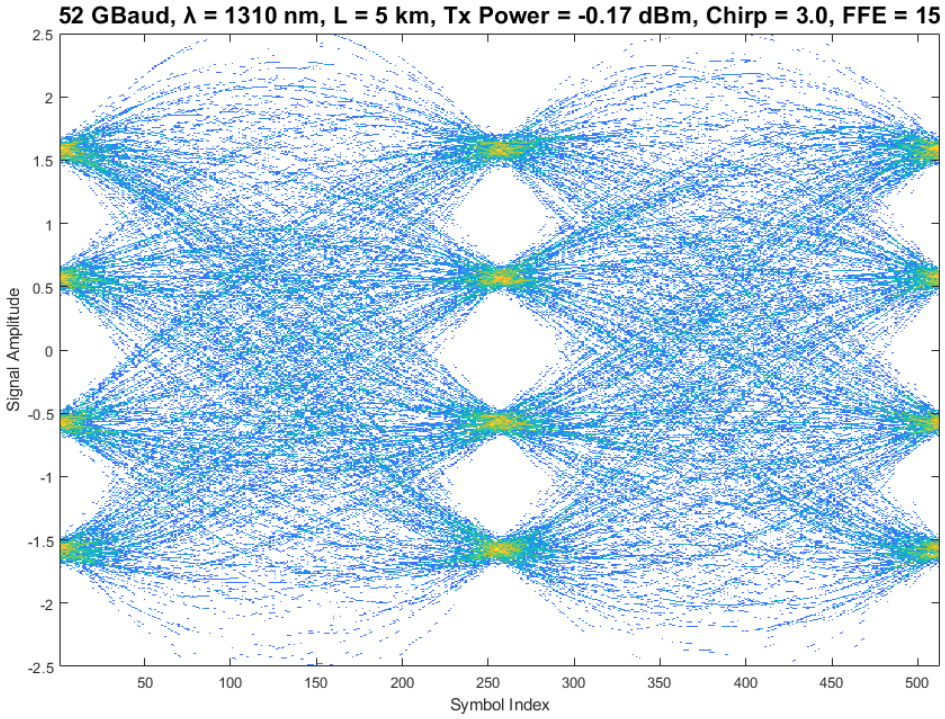

Figure 2.4: Example of an eye diagram of a PAM4 signal

- **TDECQ Measurement:** The calculate_eye_opening_and_tdecq_v2.m script implements the Transmitter and Dispersion Eye Closure Quaternary (TDECQ) metric, a standardized PAM4 performance measure central to high-speed optical fronthaul as specified in IEEE 802.3bs for 200G and 400G Ethernet and similar advanced transport standards. TDECQ quantifies the additional SNR penalty that a real transmitter-channel path introduces compared to an idealized system, translating physically observable eye closure into the extra power, or "system penalty" required to meet a stringent target BER (typically 10^{-4}), as mandated by IEEE standards. The script achieves this by analyzing received waveform samples, extracting constellation level means and statistical

percentiles from the eye diagram, and computing TDECQ as a ratio of ideal to actual modulation amplitudes. By first establishing a baseline TDECQ in a bump-to-bump (reference) scenario, subsequent measurements under real channel impairments allow for direct assessment of the incremental penalties imposed by transmitter imperfections, link dispersion, or noise. TDECQ thus serves as a critical interoperability metric for fronthaul optics, directly linking the transmitter and link quality to the error rate and margin requirements prescribed for reliable mobile fronthaul operation.

2.4.1 How TDECQ script works

The script first takes the sampled received signals at the decision points and applies K-means clustering to identify the mean voltage levels for each symbol in the PAM-4 constellation. Then it calculates statistical thresholds to define the boundaries between the decision regions. To compute eye openings, it determines the inner optical modulation amplitude (OMA) using the difference between the 1st and 99th percentile values of the highest and lowest signal levels. The outer OMA is derived from the broad spread of the entire signal distribution. TDECQ is then calculated as $20 \cdot \log_{10}\left(\frac{\text{outer OMA}}{\text{inner OMA}}\right)$ capturing how much the eye is closed due to channel impairments. We start by computing the base system "penalty" by determining TDECQ for a bump-to-bump setup (an ideal or baseline reference with minimal channel effects), and then assess additional penalties or required transmit power for the actual link.

3

Methods

3.1 MATLAB Simulation Setup

Our MATLAB simulation set-up consists of a series of interconnected modules, each representing real-world elements of an optical communication system. The simulation is modular, with each block labeled with the corresponding MATLAB scripts and surrounded by a frame indicating the physical component being simulated. The same physical component can have their aspects subdivided in different scripts modeling different phenomena (for example, a laser in an Intensity Modulated/Direct Detection (IM/DD) system can modulate directly the signal). In green we depict the modules, in blue the units, and in red the real physical component (see at page 15 Figure 3.1). Below is a description of each component:

1. **Input Generation**
   - MATLAB Scripts: `SymbolGenerator_v1`, `PatternGenerator_v1`, `Mapper_v2`
   - Simulated Physical Component: **PRBS Generator**
   - Functionality: This block generates a pseudo-random binary sequence (PRBS) used as the data source. The data is then mapped into symbol formats suitable for modulation.
2. **Drive Electronics**
   - MATLAB Scripts: `Mapper_v2`, `PulseShaper_v2`, `WaveformGenerator_v1`
   - Simulated Physical Component: **Electrical Drive Electronics**
   - Functionality: The drive electronics process the digital PRBS data into electrical drive signals. This includes pulse shaping and waveform generation to prepare the signal for digital-to-analog conversion.
3. **Digital-to-Analog Converter (DAC)**
   - MATLAB Script: `DAC_v2`
   - Simulated Physical Component: **DAC**
   - Functionality: Converts the digital electrical drive signals into analog electrical signals for direct modulation.
4. **DFB Laser**
   - MATLAB Script: `Laser_v3`
   - Simulated Physical Component: **Distributed Feedback (DFB) Laser**

- Functionality: Generates a continuous-wave (CW) optical signal, which serves as the carrier for the optical modulation process.

5. **Intensity Modulator**
   - MATLAB Script: `IntensityModulator_v2`
   - Simulated Physical Component: **Intensity Modulator**
   - Functionality: Modulates the laser's optical signal using the analog electrical signal from the DAC to produce an intensity-modulated optical signal for transmission.
6. **Fiber Optical Channel**
   - MATLAB Script: `LinChBulk_v2`
   - Simulated Physical Component: **Optical Fiber Channel**
   - Functionality: Simulates the transmission of the modulated optical signal through the fiber-optic medium, including effects such as dispersion, attenuation, and noise.
7. **Photodetector and Transimpedance Amplifier (TIA)**
   - MATLAB Script: `PD_TIA_v2`
   - Simulated Physical Components: **Photodetector and TIA**
   - Functionality: Detects the optical signal and converts it back into an electrical signal. The TIA amplifies the detected signal and then converts it from a current to a voltage signal.
8. **Equalization/Filtering**
   - MATLAB Script: `DFE_v3`
   - Simulated Physical Component: **Equalizer/Filter**
   - Functionality: Compensates for channel impairments such as inter-symbol interference (ISI) and noise. Post-processing of the received signal is performed here to retrieve the original data. In our implementation, it can work both as Feed-forward Equalizer (FFE) or a Decision Feedback Equalizer (DFE).

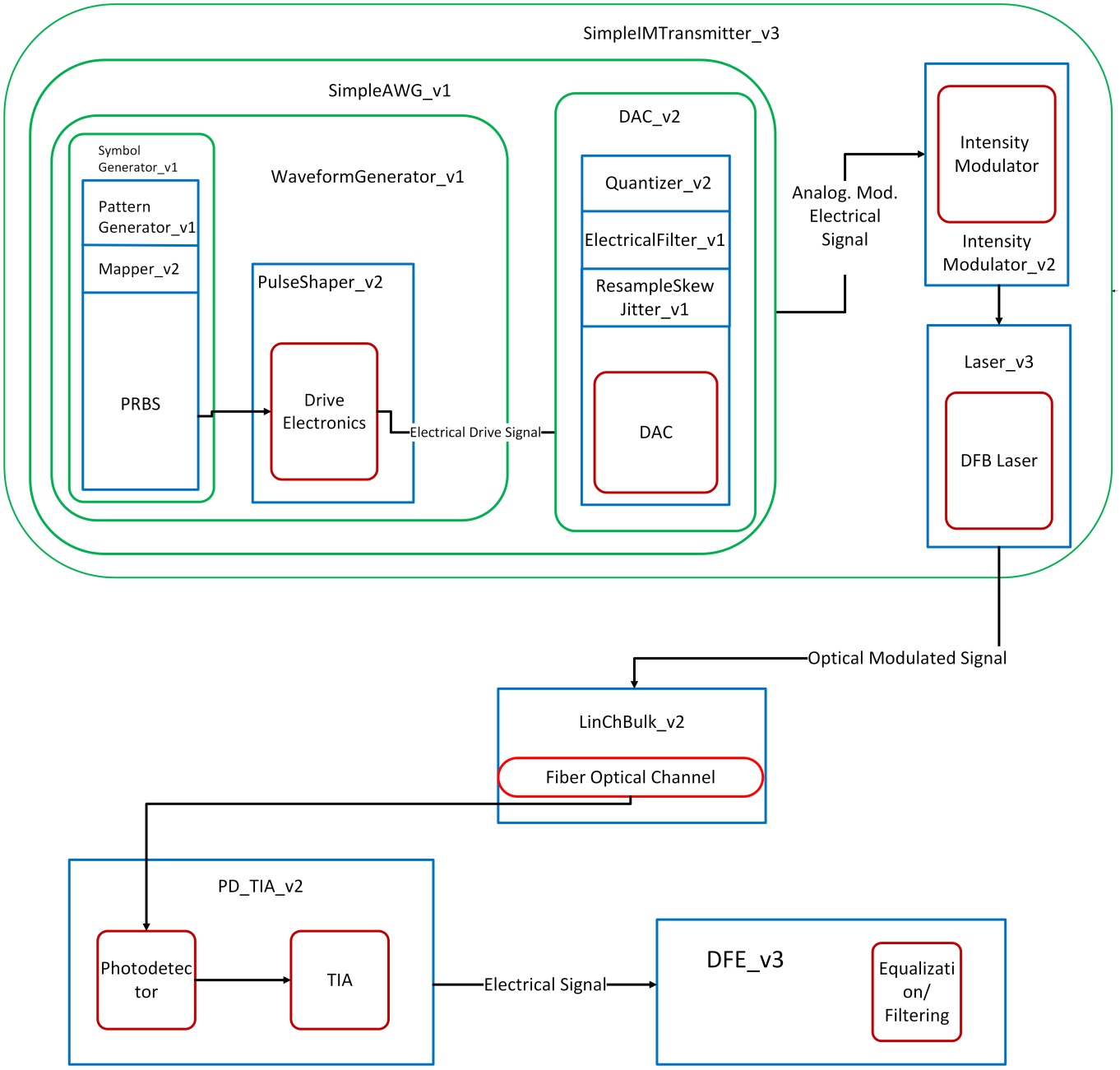

Figure 3.1: Block diagram of the simulation setup in MATALAB

3.2 Changes to the Robochameleon library

3.2.1 Chirp Model

Chirp refers to the rapid variation of the instantaneous frequency of an optical signal over the duration of a pulse. In optical communications, a pulse without chirp maintains a constant central frequency as it propagates, while a chirped pulse experiences a sweep or shift in frequency from the leading to the trailing edge of the pulse. This frequency variation can either increase with time (known as up-chirp)

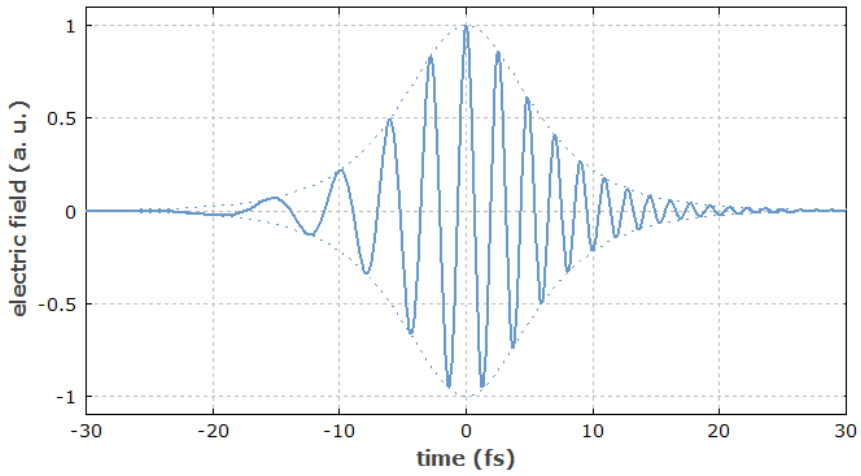

Figure 3.2: Example of strong up-chirped pulse

or decrease (down-chirp), depending on the modulation conditions. The presence of chirp is particularly important because, when such a pulse travels through a dispersive optical fiber, chromatic dispersion causes different frequency components to propagate at different speeds (group velocity dispersion) [14]. This results in pulse broadening and potentially distortion, as shown in 3.2.

The modeling of the chirp parameter within the *IntensityModulator_v2* unit is a critical and appropriate design decision for accurate simulation of real-world optical transmitters, particularly those employing Distributed Feedback (DFB) or Directly Modulated (DML) lasers[13]. In practical fiber optic communication systems, these lasers introduce significant frequency chirp during direct modulation (and to a lesser extent with external modulators) because the lasing process inherently links intensity modulation with changes in the instantaneous optical frequency. As a result, transmitted signals experience both amplitude and phase variation, with the chirped phase modulation leading to frequency shifts across the optical pulse.

Accurate capture of this effect within the transmitter model is essential for predicting how signals will broaden and distort as they propagate through dispersive fiber, potentially impacting key performance metrics such as BER, TDECQ, and eye opening. By introducing the chirp as a time-dependent phase term in *IntensityModulator_v2*, the simulation framework enables controlled studies of chirp–dispersion interaction and their impact on modulation formats such as non-return-to-zero (NRZ) and PAM4. In our simulation set-up, we resolve to an external modulator unit such as the Mach-Zehnder modulator (MZM), which solves most of the issues mentioned above but, regardless, a chirp model reveals to be useful since it can be used as a tool to pre-compensate dispersion in the fiber. This is possible because in optical fiber communications, pulse broadening occurs due to the interaction between chirp and chromatic dispersion. An optical pulse with chirp contains different frequency components that travel at different speeds through the fiber because of the frequency-dependent refractive index. The group velocity dispersion (GVD) parameter β_2 quantifies this effect, with positive β_2 (normal dispersion) causing lower

frequencies to travel faster than higher frequencies, while negative β_2 (anomalous dispersion) does the opposite[14]. Chirp pre-compensation can then apply an initial frequency chirp to the pulse with opposite sign to β_2 or, similarly, with the same sign as $D = -\frac{2\pi c}{\lambda^2} \cdot \beta_2$ which is what would then naturally occur in the fiber channel. The equation derivation for this model derives from the following relationship of chirp (α), phase (ϕ), and amplitude (E) of the optical signal [15]:

$$\alpha = \frac{\frac{d\phi}{dt}}{\frac{1}{E_{out}}\frac{dE_{out}}{dt}} \tag{3.1}$$

which defines chirp as the ratio between the phase modulation and intensity modulation of the output optical signal. We rearrange the terms,

$$\frac{d\phi}{dt} = \alpha \cdot \frac{1}{E_{\text{out}}}\frac{dE_{\text{out}}}{dt} \tag{3.2}$$

Now, since $P(t) = |E_{\text{out}}(t)|^2$ we write,

$$\frac{dP(t)}{dt} = \frac{d(E_{\text{out}}(t)^2)}{dt} = 2E_{\text{out}}(t)\frac{dE_{\text{out}}}{dt} \tag{3.3}$$

From this we can express,

$$\frac{1}{E_{\text{out}}}\frac{dE_{\text{out}}}{dt} = \frac{1}{2P(t)}\frac{dP(t)}{dt} \tag{3.4}$$

Now we can write the equation and then integrate with respect to time

$$\frac{d\phi}{dt} = \alpha \cdot \frac{1}{2P(t)}\frac{dP(t)}{dt} \tag{3.5}$$

$$\phi(t) = \int \frac{\alpha}{2}\frac{1}{P(\tau)}\frac{dP(\tau)}{d\tau} \tag{3.6}$$

$$\phi(t) = \frac{\alpha}{2}\ln|P(t)| \tag{3.7}$$

Finally, we can add the changing phase term to the modulated signal

$$E_{\text{chirped}} = E_{\text{unchirped}} \cdot \exp\left(j\phi(t)\right) \tag{3.8}$$

Listing 3.1: Chirp model addition in MZM script

```
case 'MZM'

phi = pi * ((drive.get + obj.Vbias) / obj.Vpi);
% Modulate signal based on intensity modulator output
modulatingSignal = cos(phi/ 2);

% Power management: Adjust power levels for targeted ER
Pmax = laser.P.Ptot('mW') * (cos(pi * (max(drive.get) +
   obj.Vbias) / (2 * obj.Vpi)))^2;
P0 = laser.P.Ptot('mW') * (cos(pi * (min(drive.get) + obj
   .Vbias) / (2 * obj.Vpi)))^2;
% Convert ER (dB) to linear scale
ER_linear = 10^(obj.extinctionRatio / 10);
P_offset = (Pmax - ER_linear * P0) / (ER_linear - 1);

% Apply power offset for extinction ratio and laser power
    adjustment
modulatingSig_offset = sqrt((laser.P.Ptot('mW') * (
   modulatingSignal.^2)) + P_offset);

% Modulated laser signal
unchirped_modulatedLaser = laser.fun1(@(x) x .*
   modulatingSig_offset);

% Apply chirp to the electrical field of the optical
   signal
unchirped_modulatedLaser_Pwr = abs(
   unchirped_modulatedLaser.get).^2;
chirpedSig_E = unchirped_modulatedLaser.get.* exp(1j * (
   obj.Chirp / 2) *log(unchirped_modulatedLaser_Pwr));
 modulatedLaser = signal_interface(chirpedSig_E(:),struct
    ('Fs', laser.Fs, 'P', laser.P, 'Fc', laser.Fc, 'Rs',
    drive.Rs));
```

3.2.1.1 Chirp Model Validation

To confirm the previous discussion on the chirp model, we here show a proof of the chirp behavior.

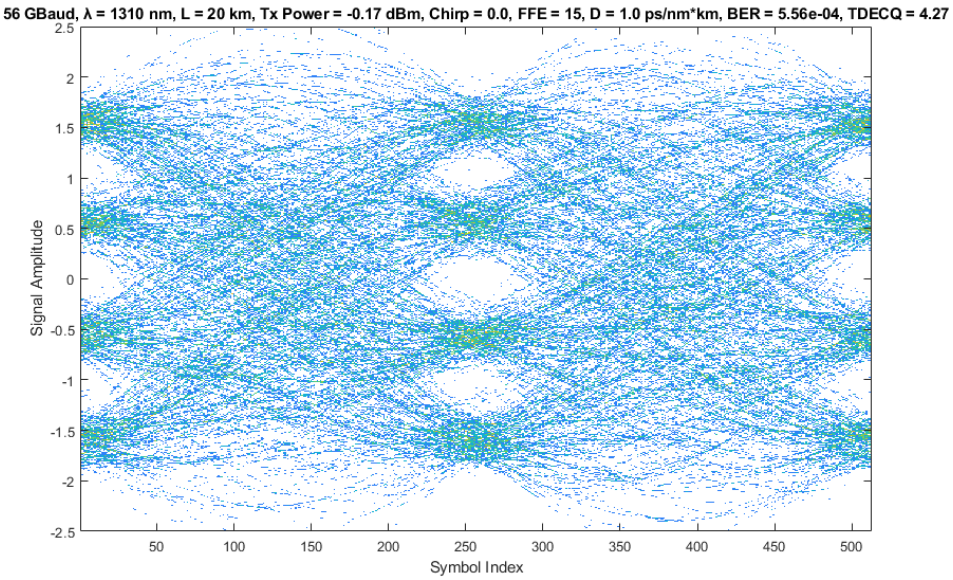

(a) No chirp applied.

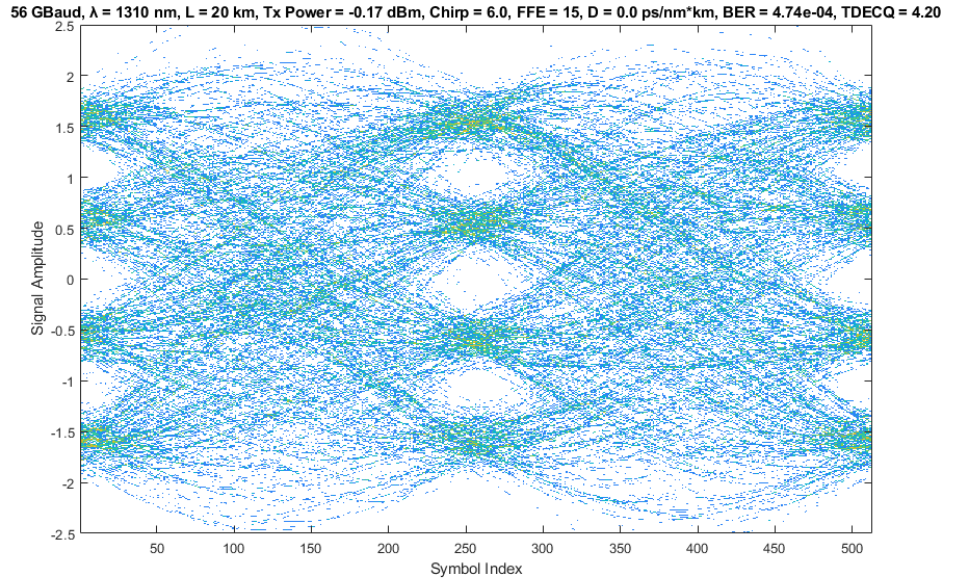

(b) With chirp, no dispersion.

Starting from a baseline case where no chirp is applied, we establish a reference value for the BER and TDECQ (Figure 3.3a).
We then observe that even setting the chirp to a relatively high value (i.e. $\alpha = 6$), while having the chromatic dispersion parameter set to zero, does not negatively affect signal, instead results in a cleaner signal due to the zero dispersion scenario (Figure 3.3b). We then try and verify that chirp, when used correctly, can effectively

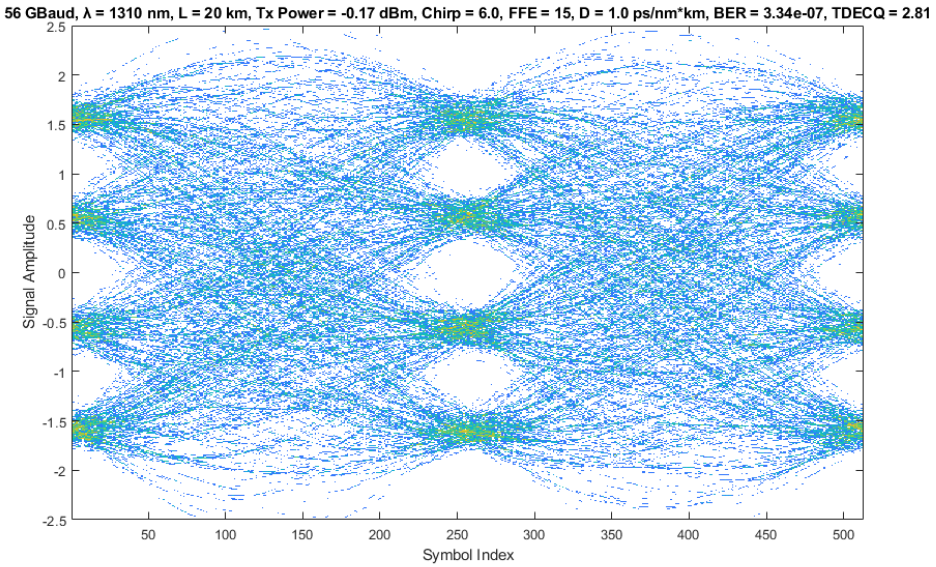

(c) Chirp compensation.

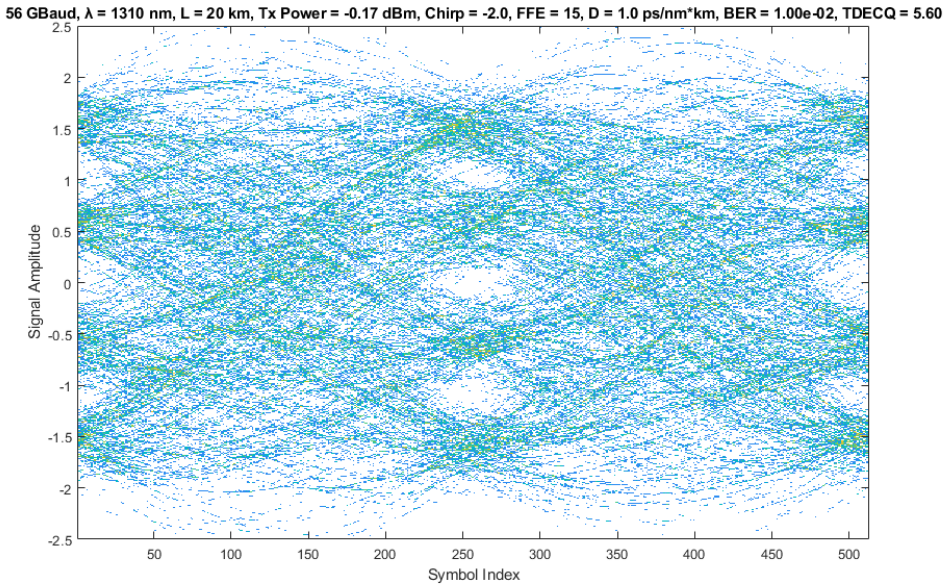

(d) Negative chirp.

Figure 3.4: Chirp Validation.

pre-compensate the dispersion. This is verified by a decrease in the TDECQ value of around 1.46 dB compared to the no chirp scenario. Finally, we test the opposite case, where the chirp and GVD parameter have the same sign and we can easily see, even for a smaller magnitude (i.e $\alpha = -2$), transmission performance exhibits a clear loss of 1.33 dB (Figure 3.4d). This behavior is coherent with the theory explained in section 3.2.1.

3.2.2 Photodiode and Transimpedance Amplifier

The second element that was modified (though not enough to be updated to a full different version) was the unit that simulates the photodetector and transimpedance amplifier (TIA).
In this model, the signal is converted from the optical domain to the electrical domain, with its performance determined by the photodetector parameters, such as its **responsivity**. Furthermore, noise contributions, including shot noise and thermal noise, are modeled and added to the resulting signal as a *signal_interface* object. Afterward, a low-pass filter is applied to simulate the bandwidth limitations imposed by electrical components, such as the TIA. To accurately represent this, a property named *TIA_BW* is introduced to model the TIA's bandwidth separately from the *Bandwidth* property, which is exclusively used for noise calculations.

Listing 3.2: Transimpedance Amplifier Parameters

```
function obj = PD_TIA(param)
            obj.Responsivity = param.Responsivity;
            obj.Bandwidth = param.Bandwidth; % For Noise
            obj.Rtherm=paramdefault(param, 'Rtherm', 50);
            obj.Idark=paramdefault(param, 'Idark', 0);
            obj.T=paramdefault(param, 'T', 290);
            obj.TIA_N_den = paramdefault(param, '
               TIA_N_den', 18e-12); % A/sqrt(Hz)
            obj.RIN = paramdefault(param, 'RIN', -145); %
                A/sqrt(Hz)
            obj.ER = paramdefault(param, 'extinctionRatio
               ', 5); % Default to 5 dB if not provided
            obj.TIA_BW = paramdefault(param,'TIA_BW', 7e9
               );  % Default to 7GHz
end
```

This separation is essential because the *Bandwidth* property represents the range over which noise is generated and integrated, reflecting the photodetector's overall noise contribution, while the *TIA_BW* property models the filtering effect of the TIA, which limits the frequencies that pass through the output. In real-world systems, the TIA often has a narrower bandwidth than the photodetector's noise bandwidth because it is designed to process only a specific range of frequencies, ensuring that high-frequency noise and unwanted signal components are suppressed. By distinguishing these two bandwidth parameters, the simulation accurately captures the physical behavior of the photodetection system, where noise is calculated

across a wide range of frequencies, but only the noise and signal within the TIA's bandwidth contribute to the final output. This approach ensures realistic modeling of the signal-to-noise ratio (SNR) and aligns with practical design practices, offering flexibility to simulate different photodiode and TIA configurations while preserving the accuracy and reliability of the results.

3.3 Printed Circuit Board Modeling

In high-speed optical communication systems, particularly those operating at data rates of 50 Gbps and beyond, the integrity of the electrical signal between components on printed circuit boards (PCBs) becomes increasingly critical. Although considerable attention is often focused on optical transmission impairments, the electrical domain, specifically the PCB traces that carry signals between electronic and optoelectronic components, can introduce significant degradation that must be carefully modeled and compensated.

At these elevated signaling rates, PCB traces no longer behave as simple conductors but rather as complex transmission lines where multiple loss mechanisms come into play. The most significant among these are dielectric losses, which occur as a result of the polarization of the substrate material under high-frequency electric fields. Conductor losses also play an important role, arising from both the skin effect and the surface roughness of the copper traces [16]. Dielectric losses are particularly problematic as they increase approximately linearly with frequency, becoming a dominant factor in signal degradation at high data rates. The loss tangent δ of the PCB material, which quantifies the dielectric's inherent dissipation of electromagnetic energy, directly impacts signal amplitude. It can also cause significant inter-symbol interference in multilevel modulation schemes like PAM4. Common PCB materials like FR4, while cost-effective, exhibit relatively high loss tangents that can limit the achievable transmission distance on board. This becomes especially critical in optical transceiver designs where high-speed electrical signals must traverse several centimeters of PCB trace between the signal-processing application-specific integrated circuit (ASIC) and the optical components.

Therefore, adding a dedicated PCB channel modeling unit to the simulation framework is useful for accurate prediction of system-level performance. This unit must account for frequency-dependent losses, impedance discontinuities, and reflections that can occur at trace transitions and vias. The model employs S-parameters derived from either electromagnetic field simulations or actual measurements of PCB channels, incorporating both magnitude and phase responses across the signal bandwidth.

For PAM4 signals, where level spacing is already reduced compared to binary signaling, these PCB-induced impairments can significantly affect receiver sensitivity and overall link performance. Moreover, the interaction between PCB channel response and any pre- or post-equalization employed in the system must be carefully considered to optimize the complete electrical-optical-electrical signal path.

By incorporating PCB effects into the simulation framework, designers can make more informed decisions about material selection, trace geometry, and component placement, as well as develop appropriate compensation strategies such as feedforward equalization (FFE) or decision feedback equalization (DFE) to mitigate these impairments. This comprehensive modeling approach becomes particularly valuable when evaluating different PCB stackup options or when determining the maximum allowable trace length for a given data rate and modulation format.

3.3.1 S-Parameter Calculation

The PCB channel modeling approach employs a differential stripline configuration with user-configurable physical dimensions and dielectric properties, represented as a 4-port S-parameter network that captures the complete electrical behavior of the differential channel. Scattering parameters (S-parameters) describe how electromagnetic energy reflects and transmits through the network at each frequency, with the 4-port configuration capturing signal coupling between the differential pair as well as reflections and transmissions at both ends of the channel. This frequency-domain characterization provides a complete linear description of signal propagation, making it ideal for predicting how high-speed digital signals will behave as they traverse the transmission line structure.

At high-speed signaling rates, particularly those exceeding 25 GBaud, the wavelength of the highest frequency components becomes comparable to or smaller than the PCB structure dimensions. This necessitates extremely fine meshing in EM simulations to accurately capture field behavior. For instance, 50 GBaud PAM4 signaling, with each symbol carrying 2 bits, yields a Nyquist frequency of 25 GHz. However, significant frequency components extend to approximately 37.5 GHz (1.5× Nyquist) to accurately represent signal transitions, resulting in wavelengths of less than 2 mm in typical PCB materials and requiring mesh elements of 350 micrometers or smaller.

This fine meshing creates substantial computational complexity since mesh elements scale cubically as element size decreases across all three dimensions. The electromagnetic solver must then compute field interactions between all elements, generating large matrices solved at each frequency point. Although MATLAB's S-parameter calculation methods employ various numerical techniques to handle these matrices, the computational burden remains significant, especially for longer trace lengths where mesh element count increases proportionally.

Our implementation addresses this challenge through a simple but effective approximation: instead of calculating S-parameters for the entire trace length, we compute parameters for a shorter reference trace and extend the results using complex propagation constants γ.

The function is implemented as follows:

- Call the S-Parameter method for a shorter trace [3.5a]

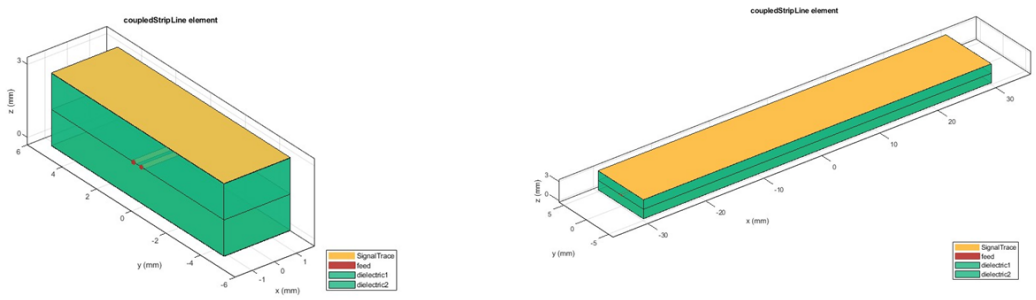

(a) Trace of 3 mm length **(b)** Trace of 6 cm length

Figure 3.5: Side-by-side representation of traces of different lengths.

- Extract the module and phase from the forward transmission coefficient (S_{21})

$$||S_{21}|| = e^{-\alpha L}, \angle S_{21} = -\beta L$$

  where L is the shortened length.
- We write the propagation constant

$$\gamma = \alpha + j\beta$$

- Compute the extension factor like:

$$Extension = e^{-\gamma \Delta L}$$

  where ΔL is the difference in distance between the two traces.
- Multiply the matrix of S-Parameters by extension factor to obtain the values for the longer trace

Additionally, the S-Parameters are computed across a vector of frequencies that is user defined thanks to a function called "frequencygrid" that efficiently computes a selected range of frequencies based on the input symbol rate:

- **Low Frequencies** (1 MHz - 0.4×fNyquist) 15 points: Captures fundamental behavior and DC characteristics
- **Mid-band** (0.4×fNyquist - 0.9×fNyquist) 40 points: Tracks transition to high-frequency effects
- **Nyquist Region** (0.9×fNyquist - 1.2×fNyquist) 70 points: Highest resolution where most critical signal components exist
- **Extended Band** (1.2×fNyquist - 2.1×fNyquist) 40 points: Captures harmonics and validates filter response

This distribution, totaling approximately 165 points across the spectrum, provides optimal computational efficiency while ensuring accurate characterization of the channel's frequency response, with emphasis on the critical Nyquist region where signal integrity issues are most likely to manifest.

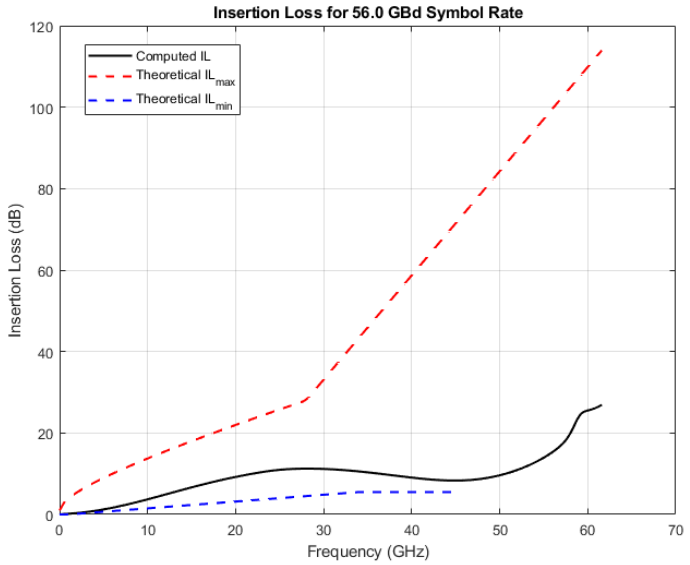

Figure 3.6: Insertion Loss plotter for PCB objects

3.3.2 Diagnostics for the electrical channel

Since optical-communication standards impose tight requirements on both performance and interoperability, the electrical interfaces in optoelectronic transceivers are just as important as the optical parts. For over 25 years, the Optical Internetworking Forum (OIF) has led the way by publishing whitepapers and implementation agreements that lay out guidelines for electrical-channel designs, connector specifications, and high-speed signaling requirements. For this reason, in this thesis we developed an additional script, outside the Robochameleon's framework, to compare our PCB-level channel model to these industry-approved standards.

In this case, the test scenarios are confined to the 36.0–58.0 GBaud range, in accordance with the requirement laid out in Section 27 of the OIF CEI-05.2 specification [17].

Using the formulas for minimum and maximum theoretical Insertion Loss (IL):

$$IL_{\max} = \begin{cases} 0.998 + 2.397\sqrt{\frac{f\times 58}{f_b}} + 0.486\frac{f\times 58}{f_b}, & f_{\min} \le f \le \frac{f_b}{2} \\ -43.63 + 2.47\frac{f\times 58}{f_b}, & \frac{f_b}{2} < f \le 0.8 f_b \end{cases} \tag{3.9}$$

$$IL_{\min} = \begin{cases} 0, & f_{\min} \le f \le 1\text{GHz} \\ \frac{1}{6}(f-1), & 1\text{ GHz} < f \le 34\text{GHz} \\ 5.5, & 34\text{GHz} < f \le 0.8 f_b \end{cases} \tag{3.10}$$

where f_b is the signal rate.

We can create a plotting function for the insertion loss for each PCB object we generate in Robochameleon by calling "OIF_CEI_05_2(PCB)" where "PCB" is the variable referencing the PCB object.

3.4 Key Parameters for simulation

The simulation framework allows for a multitude of parameter choices ranging from symbol pattern generation, digital signal design, electrical, and optical components. Here we list the main ones used for an IM/DD communication setup.

Transmitter			
Name	**Parameter**	**Value**	**Comment**
Modulation Order	M	4	4 symbol constellation
Modulation Format	modulationFormat	ASK	Here it's equivalent to PAM
Signaling speed	symbolRate	$28/56/112 \cdot 10^9$	This is [Baud], not [bit/s]
Wavelength	lambda	$1310 \cdot 10^{-9}$	Zero-dispersion wavelength
Num. Simulated Bits	lengthSequence	$3 \cdot 10^6$	Balance precision/time
Extinction Ratio	extinctionRatio	5	$\frac{P_{max}}{P_{min}}$ in [dB]
Shaping Technique	pulseShape	NRZ	other options like RC, RRC, RZ
Minimum OMA (Optical Modulation Amplitude)	MinOMA	0	Value in [dBm], uses then extinction ratio to compute the laser power

Table 3.1: Key simulation parameters for the transmitter.

In the transmitter, the OMA parameter does not directly combine with the laser input but it is hard coded instead using the relationship with the extinction ratio.

$$OMA = 2P_{av}\frac{r_e - 1}{r_e + 1} \tag{3.11}$$

We extract P_{av} and use it for the power input *laser.Power*:

$$P_{av} = \frac{OMA}{2} \cdot \frac{r_e + 1}{r_e - 1} \tag{3.12}$$

where r_e is the extintion rate in linear scale ($10^{param.extinctionRatio/10}$).

Channel			
Name	**Parameter**	**Value**	**Comment**
Fiber length	ch.L	10/15/20	Length in [Km]
Dispersion Parameter	ch.D	[0;5]	Using fiber SMF-28, used value for 1310 nm, $[ps/nm \cdot km]$
Dispersion Slope	ch.S	≤ 0.092	Using fiber SMF-28, used value for 1310 nm, $[ps/nm^2 \cdot km]$
Attenuation	ch.loss	0.4	Loss in [db/Km]

Table 3.2: Key simulation parameters for the channel.

The linear fiber optic channel model implemented in LinChBulk_v2 provides a comprehensive yet efficient framework to simulate the key physical effects encountered during the optical signal transmission in fiber networks. This model is built to mimic linear fiber behavior as closely as possible, especially for standard single-mode fiber (SMF-28). The fiber length (ch.L) essentially sets how far the signal travels through the fiber; in our typical simulation scenarios, we examine lengths of 10, 15, or 20 kilometers. The longer the fiber, the more pronounced the cumulative effects of dispersion and loss become.
Dispersion, which causes different wavelengths to spread out as they propagate, is primarily characterized by the dispersion parameter (ch.D). This value, measured in ps/(nm $\cdot$ km), can be positive or negative depending on the fiber and operating wavelength; for SMF-28 at 1310 nm, values typically fall within the range of 0 to 5. Closely related is the dispersion slope (ch.S), representing how the dispersion itself varies with wavelength, and for SMF-28 at 1310 nm, values do not exceed 0.092 ps/(nm^2 $\cdot$ km). Both of these parameters are important for accurately capturing pulse broadening and other chromatic dispersion effects over long distances.

During signal propagation simulation, the process begins with polarization and mode mixing, followed by chromatic dispersion and polarization mode dispersion (PMD), and finally, signal loss is accounted for based on the fiber's attenuation. Default values and lookup tables embedded in the script ensure that, unless otherwise specified, realistic SMF-28 fiber behavior is assumed, making the model readily applicable for a broad range of wavelength and system configurations without user input. By adjusting these principal parameters, it is possible to explore and analyze the impact of real-world fiber characteristics on optical signal transmission, allowing for robust and flexible evaluation of communication system designs under various practical conditions.

Receiver			
Name	**Parameter**	**Value**	**Comment**
Photodetector Responsivity	pd.Responsivity	0.7	4 symbol constellation
Bandwidth	pd.TIA_BW	0.6*symbolRate	Assuming a receiver with 60 % bandwidth of signal speed
Tempetature	pd.T	350	Temperature used for noise calculations in Kelvin
FFE Taps	DFE.numFFTaps	7-15	Number of feed-forward taps depending on standard
DFE Taps	DFE.numFBTaps	1	Number of feed-back taps

Table 3.3: Key simulation parameters for the receiver.

The receiver architecture, as implemented in the PD_TIA, DCblock_v1, and DFE_v3 units, follows a typical signal processing sequence encountered in optical communication systems. The photodiode and transimpedance amplifier (PD_TIA) first convert the optical input to an electrical signal, with responsivity and bandwidth parametrization directly reflecting practical device specifications. Notably, the simulation accounts for thermal noise effects by including an explicit temperature parameter, thereby aligning with standard noise modeling approaches.
Following signal conversion, the DCblock_v1 stage serves to suppress any direct current (DC) component in the signal. This step is necessary to mitigate potential baseline drift or offset that may accumulate due to preceding stages or noise effects. The model provides flexibility in the scope of DC removal, supporting both per-channel and per-polarization blocking modes depending on simulation requirements.
The signal finally proceeds to the DFE_v3 module, which is configured as a decision feedback equalizer. Here, the number of feed-forward and feedback taps is selected according to the anticipated level of inter-symbol interference and the modulation format. By appropriately configuring these parameters, the model enables a realistic representation of post-detection equalization in fiber optic communication links.

4

Results and Discussions

The general approach for which the simulations have been carried out consists of the following stages:

- Establish the standard to be simulated.
- Isolate the varying parameter to study its impact.
- Plot the results to better visualize the data.

4.1 Case study: 200GBASE

In the course of this simulation for a signaling speed of 112 Gbaud PAM4 we span across three different reach: 10, 15 and 20 km. We assume the same model as described in Figure 3.1, meaning that the signal does not traverse the PCB unit. This is done by assuming the transceivers used are in the linear pluggable optics (LPO) category. This essentially means that the optical modules do not include retimers or DSPs; instead, they rely on the host ASIC to generate and recover high-quality signals directly. Since there is no reconditioning of the electrical signal within the module, the assumption of LPO inherently excludes the modeling of PCB trace distortions. These distortions would typically degrade signal integrity beyond what a linear module can tolerate without host-side compensation. As a result, LPO designs are best suited for architectures with minimal electrical channel impairments. This includes those enabled by short-reach electrical connections or co-packaged optics, where clean signal conditions can be guaranteed by the system layout [18].

4.1.1 Chirp compensation

The first element we inspect is the chirp value added in the transmitter for pre-compensating for the effects of chromatic dispersion that arise in the channel model. We first run the simulations over a span of 10 different dispersion coefficients ranging from 0.1 to 1 $ps/nm \cdot km$, and for each coefficient, we try to pre-compensate with different values of chirp α.

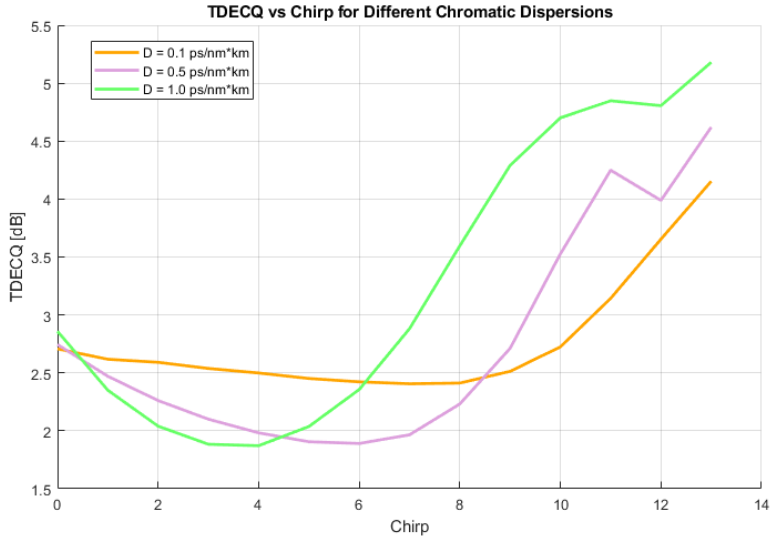

Figure 4.1: Chirp comparison for 200GBASE and 10 Km

For this simulation case, we use TDECQ as measurement given that BER, when chromatic dispersion is compensated, reaches very small (in the order of 10^{-7}) or zero values and fluctuates due to the random input bit sequence that changes at each iteration. From the plot, we can see that for higher dispersion coefficients chirp compensation is achieved for lower values but tends to quickly overcompensate and degrade performance past the initial result with no chirp. This is consistent with the nature of the chirp-dispersion interaction: when the transmitter chirp and the channel dispersion are properly matched, the temporal broadening caused by dispersion can be partially canceled by the frequency shift introduced by the chirp. In this regime, the signal pulse at the receiver can actually become narrower than in the uncompensated case, resulting in a more opened eye diagram and a lower TDECQ. This effect explains why, for certain chirp values, the higher dispersion cases (such as 1 ps/nm $\cdot$ km) can achieve a lower minimum TDECQ than the low-dispersion case (0.1 ps/nm $\cdot$ km), where such interplay is minimal and the TDECQ remains relatively flat. However, as the chirp increases beyond the optimal point, the combined effects quickly become detrimental, leading to increased eye closure and a sharp increase in the TDECQ curve.

As the fiber length increases to 20 km, the total accumulated chromatic dispersion grows proportionally, shifting the optimal point for chirp compensation. In this case (Figure 4.2), the intermediate dispersion coefficient of 0.5 ps/nm $\cdot$ km achieves the lowest TDECQ for an appropriate value of chirp, outperforming both the lowest and highest dispersion cases. This indicates that when the overall dispersion becomes too large, as for D = 1.0 ps/nm$\cdot$km at 20 km, the beneficial effect of chirp compensation diminishes and eventually leads to increased distortion and eye closure. Therefore, the optimal balance between chirp and chromatic dispersion for minimizing TDECQ is not fixed, but depends on the total length of the optical link.

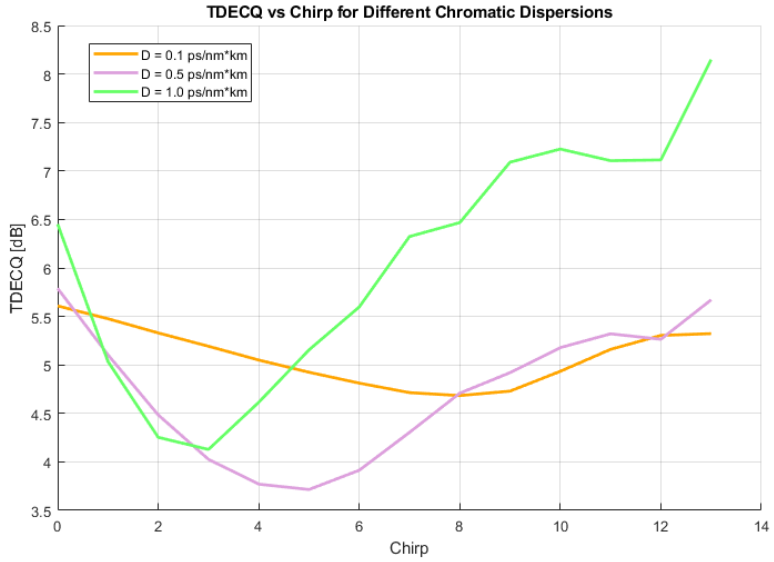

Figure 4.2: Chirp comparison for 200GBASE and 20 Km

4.1.2 Number of Feed-forward taps in the equalizer

Another useful deployment of the simulation framework is to investigate the effect on the received signal when modifying the number of feed-forward taps in the equalizer.

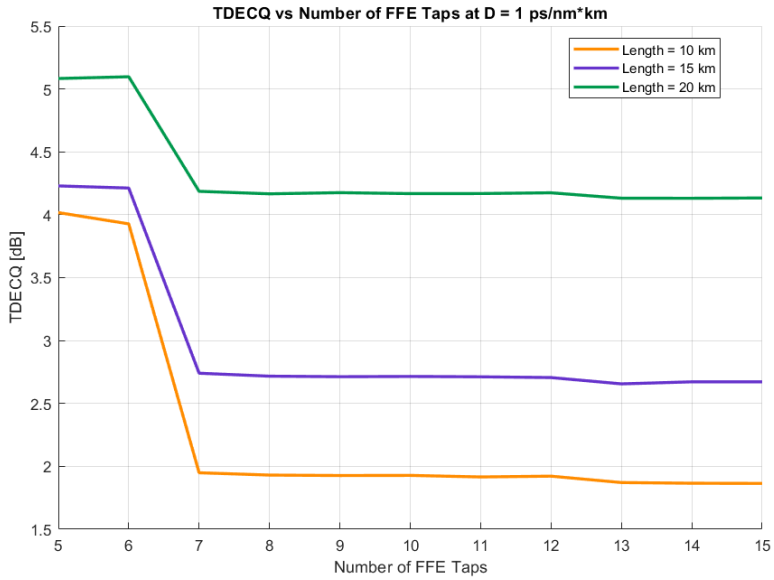

Figure 4.3: Comparison for different FFE taps for 200 GBASE at different fiber lengths

The simulation results, shown in Figure 4.3, indicate that increasing the number of FFE taps leads to a marked improvement in TDECQ up to about seven taps, after which further increases do not yield substantial performance gains and the TDECQ curve saturates. This trend is consistently observed across all fiber lengths

considered. Although the absolute TDECQ value rises with increased transmission distance due to greater accumulated dispersion, the number of taps required to mitigate inter-symbol interference remains nearly constant. This suggests that the dominant ISI caused by chromatic dispersion is effectively compensated for within the first several taps of the equalizer, regardless of fiber length or span. Additional taps do not contribute meaningfully once this channel memory is covered. Covering the channel memory means that the equalizer's tap span is sufficient to cover the temporal spread of the channel's impulse response. This temporal spread is determined primarily by chromatic dispersion.

4.2 Case study: 100GBASE

This simulation framework was designed to isolate and analyze electrical channel impairments by implementing a short fiber link with minimal chromatic dispersion and chirp effects. This configuration allows for focused examination of the PCB transmission line characteristics and their impact on high-speed PAM4 signaling, without the additional variables introduced by fiber-optic propagation effects. The controlled setup provides clear visibility into how electrical interconnects degrade signal integrity in 100+ Gbps optical communication systems and become major bottlenecks. For this reason we set the transmission distance between 500 m and 2 km and set both the dispersion parameters and chirp to zero.
For our PCB we start by picking the physical dimensions for the traces to have a resulting differential impedance (Z_d) of around 100 Ω which is a typical value for digital signal transmission.

Parameter	**Value**
Trace width (w)	300 μm
Trace spacing (s)	130 μm
Trace thickness (t)	150 μm
Trace length (l)	3 cm
Dielectric thickness (2h + t)	1.45 mm
Dielectric relavtive permittivity (ϵ_r)	3
Dielectric Loss-tangent (tanδ)	0.003

Table 4.1: PCB design parameters

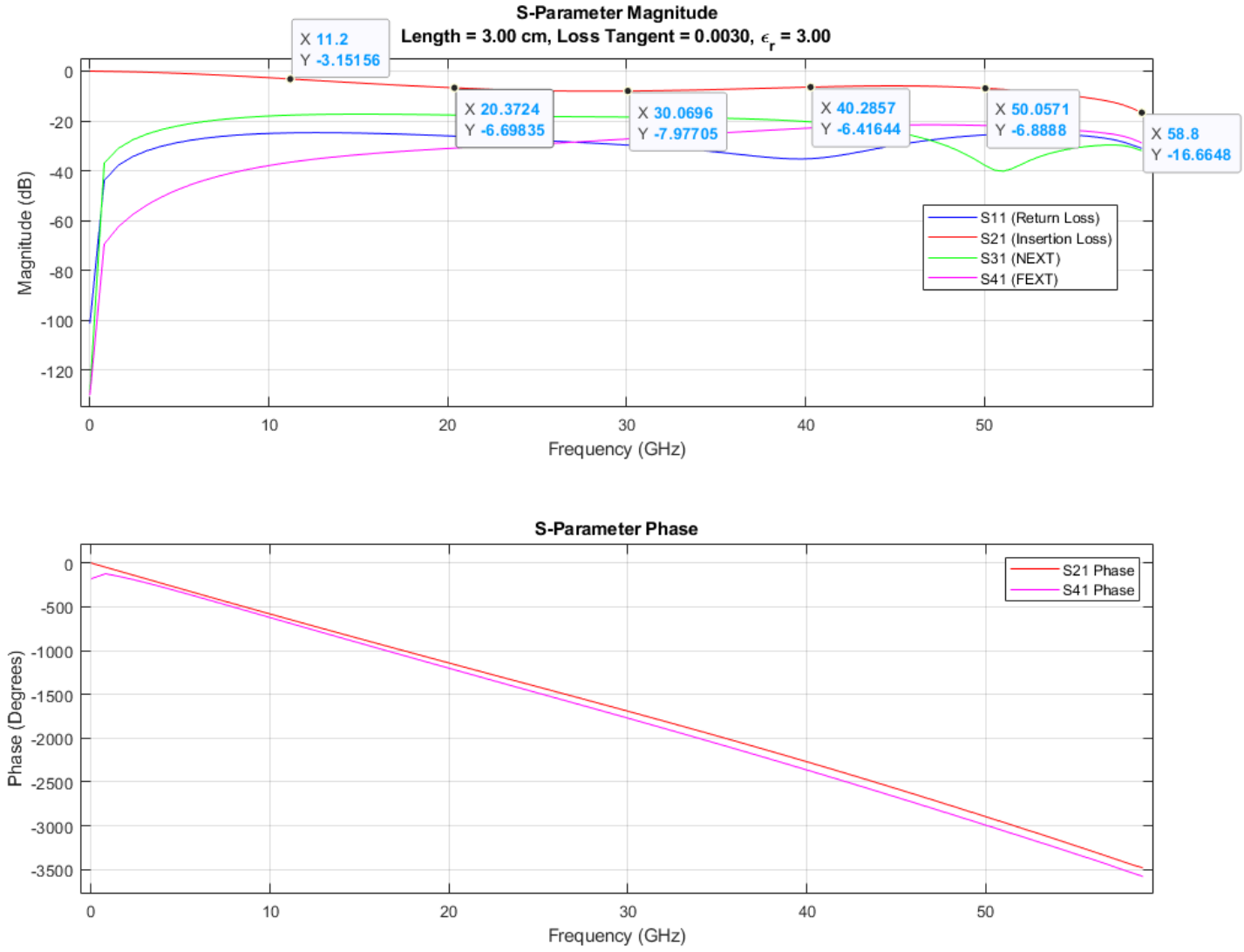

Figure 4.4: Plot of magnitude and phase of S-parameters

To find appropriate test values, the approximated formulas of Institute of Printed Circuits (IPC) 2141 were used to find the odd (Z_o) and differential impedance(Z_d):

$$Z_o \approx \frac{60}{\sqrt{\epsilon_r}} \cdot ln\left(\frac{1.9(2h+t)}{0.8w+t}\right) \tag{4.1}$$

$$Z_d \approx 2Z_o\left[1 - 0.347\exp\left(-2.9\frac{s}{2h+t}\right)\right] \tag{4.2}$$

Once we compute the S-parameter, we see that the measured insertion loss (S_{21}) demonstrates progressive frequency-selective attenuation, starting with minimal loss at DC and increasing to approximately 3 dB already at 11 GHz and almost 7 dB at 20 GHz. The channel maintains relatively stable performance through the 28-30 GHz region with losses around 8 dB, before showing more substantial degradation

at higher frequencies, reaching approximately 17 dB at 59 GHz. This channel is in line with the standardization mentioned in the OIF documentation [17] as shown in Figure 4.5.

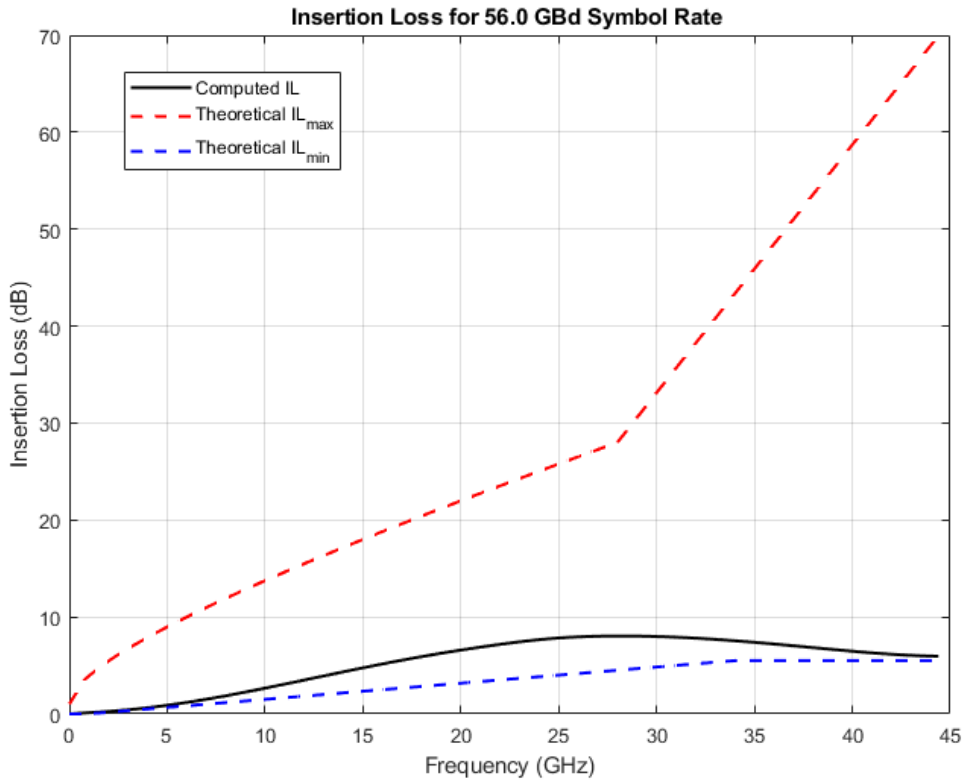

Figure 4.5: Insertion Loss for the tested trace

It is important to note that the curve adheres well to the lower limit, especially in the higher frequency range. This is due to the fact that our model is much simplified from a real PCB complete of vias, active components, and more complex geometries. This frequency-selective behavior creates a low-pass filtering effect that distorts the sharp transitions required for reliable PAM4 level discrimination, resulting in significant ISI. The relatively linear phase response across the frequency range indicates consistent group delay characteristics, suggesting that the primary impairment mechanism is amplitude distortion rather than timing skew. These combined effects contribute to the substantial signal degradation observed in time-domain measurements, where the clear four-level PAM4 eye patterns become severely degraded with complete eye closure, making direct symbol detection difficult without equalization. The implemented 10-tap Feed-Forward Equalizer (FFE) attempts to compensate for the channel's frequency-selective losses through inverse filtering. By applying high-frequency emphasis that counteracts the PCB's low-pass characteristics, the FFE aims to restore the original signal spectrum and recover the PAM4 eye openings. The frequency response $|H^{-1}|$ (Figure 4.7) of the optimized FFE shows the expected high-frequency gain of approximately 20+ dB, designed to compensate for the corresponding channel losses. However, this aggressive equalization approach

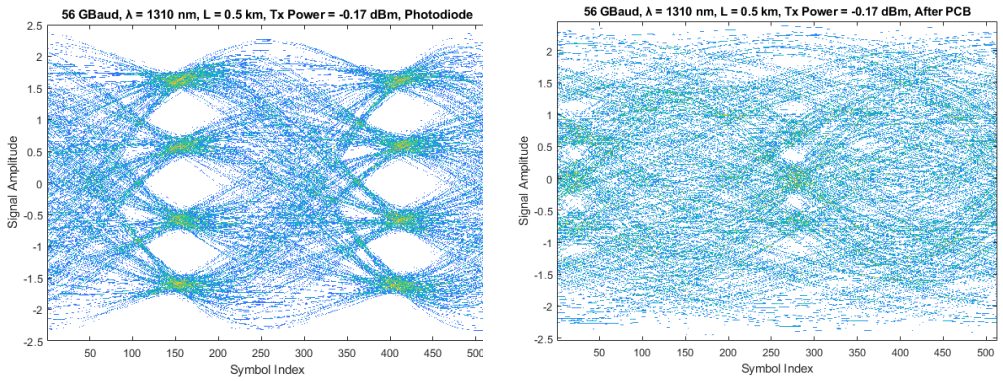

(a) **(b)**

Figure 4.6: Eye diagrams of the signal before (a) and after (b traversing the PCB trace

inherently amplifies both signal and noise components, leading to a fundamental trade-off between ISI reduction and signal-to-noise ratio degradation.

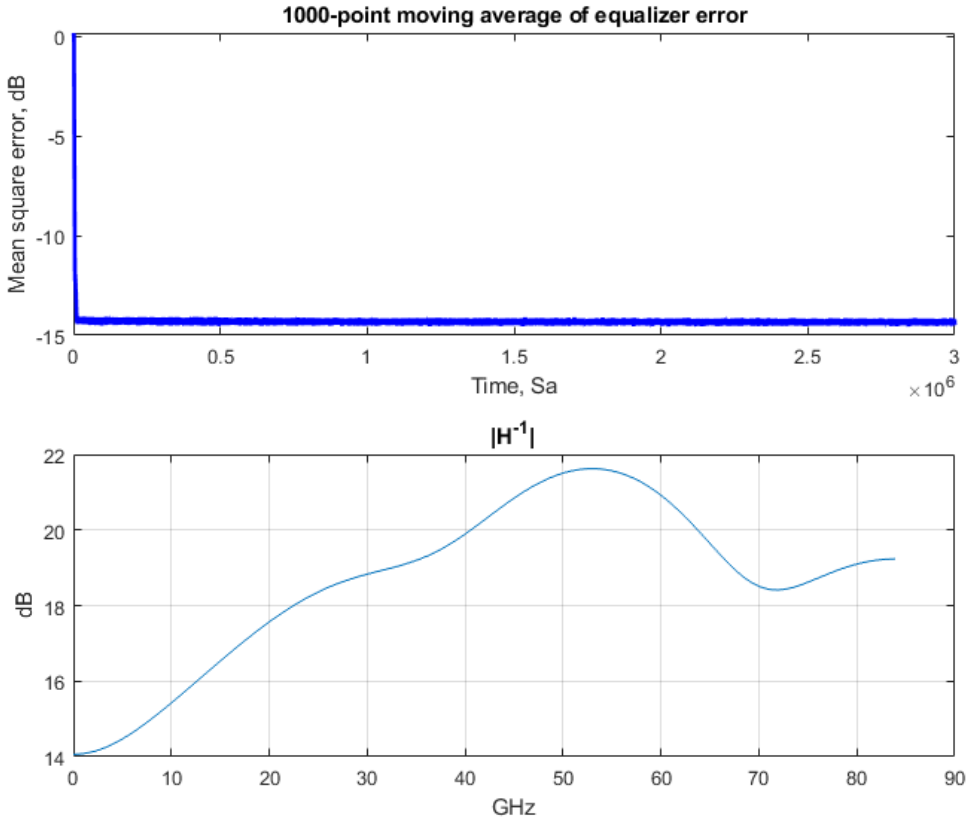

Figure 4.7: FFE performance metrics

Now, when looking at the post equalization resulting eye diagram (Figure 4.8), we can observe both the potential and limitations of linear FFE compensation. While

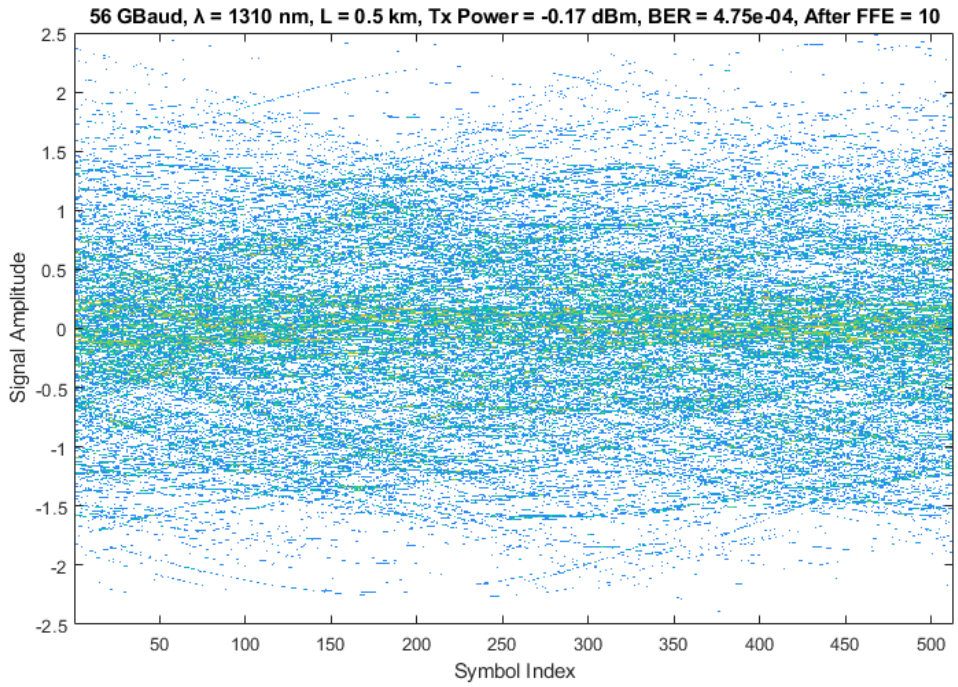

Figure 4.8: Eye diagram after equalization with unrecognizable levels

the system achieves a measurable bit error rate of 4.75×10^{-4} through symbol-level detection as implemented in the BER counter unit, the eye diagrams remain severely degraded, with no discernible eye openings. This apparent contradiction highlights that statistical symbol detection can function even when eye diagram analysis suggests prominent signal failure. However, the noise-dominated characteristics of the equalized signal indicate that the FFE has reached its compensation limits, transforming severe ISI into amplified noise. These findings demonstrate the critical need for advanced channel compensation techniques in high-speed optical systems. The linear FFE approach, while providing some signal recovery, cannot adequately address channels with severe frequency-selective impairments without unacceptable noise enhancement. For this reason, additional components such as a continuous-time linear equalizer (CTLE) before the FFE could provide initial high-frequency peaking with lower noise amplification.
Additionally, we can run the simulation for multiple lengths of the same PCB model and notice that the limit for acceptable error rates (already at 1.23×10^{-3} at 4 cm) gets easily crossed in the absence of the aforementioned DSP components.

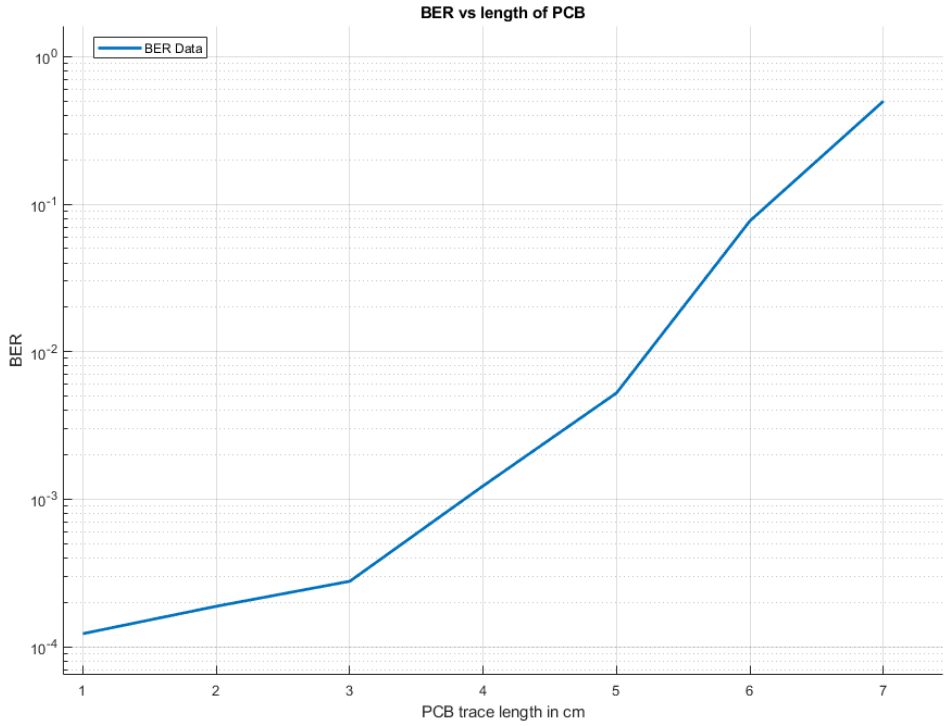

Figure 4.9: BERs for incresingly longer PCB traces

5

Conclusion

5.1 Summary of main outcomes

This thesis explored the application of the Robochameleon MATLAB framework to model and analyze optical communication links in mobile fronthaul systems, with a focus on high-speed standards such as 200GBASE-LR and 100GBASE-LR. Employing a modular approach, the simulation framework accurately replicated key components of optical communication systems, including the transmitter, channel, and receiver. Key achievements included the successful integration of a chirp model in the intensity-modulated transmitter for pre-compensation of chromatic dispersion and the implementation of a printed circuit board (PCB) model that accounted for high-frequency losses and differential transmission. Extensive simulations demonstrated the effectiveness of these models in analyzing performance through parameters such as Bit Error Rate (BER), Eye Diagrams, and Transmitter and Dispersion Eye Closure Quaternary (TDECQ). The project verified that pre-compensating with chirp significantly reduced dispersion penalties and that the impact of PCB-based losses should be analyzed comprehensively, providing critical insights into system bottlenecks for next-generation optical communication systems.

5.2 Reflections on approach and methods

The modular structure of the simulation framework proved to be highly effective, allowing isolated examination of channel and component-specific impairments. The Robochameleon library's flexibility enabled seamless integration of newly developed modules without disrupting the simulation pipeline. The accurate representation of system-level effects and their decomposition into measurable parameters like BER and TDECQ exemplified the method's validity. However, challenges were encountered that impacted the implementation. First, the system memory requirements for MATLAB and the high computational intensity of S-parameter extractions for PCB traces restricted the simulation of more complex/non-uniform boards. Second, the absence of real measured data for verification meant that simulated outcomes, though aligned with theoretical expectations, could not be benchmarked against experimental results. Finally, the exclusion of certain effects, such as power consumption and detailed temperature modeling in the optical channel, meant that many real-world effects could not be explored.

5.3 Unexpected results and considerations

While the outcomes largely matched theoretical predictions, there were some unexpected or less favorable results. For example, the linear FFE displayed limited effectiveness in recovering signals degraded by severe PCB losses. Even with increasing number of taps, the eye diagrams remained substantially closed, underscoring that FFE alone is insufficient in realistic high-loss cases. This revealed the critical importance of including additional unit implementing equalization techniques such as Continuous Time Linear Equalizers (CTLE) to optimize system performance. Another unexpected result was the statistical detection capabilities revealed by the BER counter in cases of closed eye diagrams. Although signal integrity appeared poor visually, the robust BER performance highlighted the potential of higher-layer processing in recovering degraded signals, presenting an area for future exploration.

5.4 Closing remarks

In conclusion, this project presented a simulation framework capable of addressing system-level and component-level challenges in next-generation optical communication systems. While some limitations and challenges were encountered, the framework demonstrated robust capabilities for analyzing and optimizing core components of high-speed fronthaul systems. Real-world testing could help validate or correct the models developed in this framework, ensuring greater correlation between simulated results and practical performance. The modular and extensible nature of the simulation strategy paves the way for its application across varied scenarios and for future advancements in optical network design and deployment. Further development of this framework could incorporate additional effects, such as thermal impacts, power consumption, more complex channels, making it a more reliable and comprehensive tool for the designing and research of future mobile communication networks.

6
Future Works

The optical communication simulation framework developed in this project establishes a foundation for comprehensive system modeling, with potential for expansion and enhancement across multiple use cases. This chapter outlines examples for future development that would advance the capabilities and practical applicability of this simulation environment.

6.0.1 Framework extension for mobile optical networks

The Robochameleon framework provides a comprehensive approach to optical communication system modeling, offering a foundation that extends beyond the scope of this current implementation. This MATLAB-based framework enables modeling and simulation of various components in mobile optical networks, including coherent detection systems, advanced modulation formats, and network topologies. Future development could leverage Robochameleon's modular architecture to implement wavelength division multiplexing (WDM) systems, coherent optical transmission, and digital signal processing algorithms. The framework's capability to handle long and complex simulation chains makes it suitable for modeling fronthaul and backhaul networks in 5G and future 6G mobile communications. Additionally, given the agnostic approach on the simulated signals, this framework could be extended to simulate other transmission media such as free-space optical communications, underwater optical networks, and satellite communication links, addressing various optical communication scenarios relevant to mobile networks.

6.0.2 Evolution of PCB model

The current PCB model implementation presents opportunities for enhancement towards a more realistic system representation. Frequency-dependent tangent loss modeling should replace the current constant loss assumptions, providing more accurate high-frequency behavior for high-speed optical communication systems operating at 50 Gbps and beyond. The incorporation of vias modeling represents a necessary addition, as these interconnects significantly impact signal integrity at high frequencies. Future implementations should include modeling of differential via pairs, blind and buried vias, and via stitching effects to capture the electromagnetic behavior in multilayer PCB structures. But given the hardware limitations already discussed in Section 3.3.1, a more clever approach would be to create a comprehensive S-parameter database containing pre-characterized PCB components and structures. This database would include various trace geometries, via configurations,

connector models, and component footprints, enabling rapid simulation designing without requiring electromagnetic simulations for each component.

6.0.3 Additional units

The current simulation framework would benefit from the addition of signal processing components commonly found in modern optical communication systems. Continuous Time Linear Equalizers (CTLE) would enable more accurate modeling of receiver-side equalization, particularly for compensating high-frequency losses in the electrical domain.
Pre-emphasis functionality on the transmitter side would provide modeling of signal conditioning techniques used to overcome channel limitations. This includes feed-forward equalization (FFE), decision feedback equalization (DFE), and adaptive equalization algorithms that adjust parameters based on channel conditions.

Bibliography

[1] R. Borkowski, E. Porto Da Silva, S. Gaiarin, M. Iglesias, M. Piels, D. Zibar, R. Jones, J.C. M. Diniz, X. Pang, O. Ozolins, L. Marcon, "Robochameleon MATLAB Framework", 2016. [Online]. Available: https://github.com/dtu-dsp/Robochameleon

[2] IEEE, "IEEE 802.3 Ethernet Working Group" Available: https://www.ieee802.org/3/index.html

[3] E. Trojer, V. Skogman, A. Olsson, T. Thyni, M. Forsman, J. Österling, D. Cederholm, M. Berg, and R. Stake, "Packet fronthaul – design choices towards versatile RAN deployments," Ericsson White Paper, EAB-21:006051 Uen, Aug. 2021. [Online]. Available: https://www.ericsson.com/4a3788/assets/local/reports-papers/white-papers/08162021_packet_fronthaul.pdf

[4] E. Trojer, V.Skogman, A. Olsson (2021). "Packet Fronthaul: Design Choices for 5G Networks" Available: https://www.ericsson.com/4a3788/assets/local/reports-papers/white-papers/08162021_packet_fronthaul.pdf

[5] R. Pérez-Aranda, B. Grow "802.3cz PHY naming", IEEE 802.3cz Task Force, Nov 2020 Plenary. Available: https://www.ieee802.org/3/cz/public/nov_2020/perezaranda_3cz_02c_1120_phyname.pdf

[6] Ericsson, "Ericsson Mobility Report," Stockholm, Sweden, Nov. 2024. [Online]. Available: https://www.ericsson.com/mobility-report [Accessed: May 2, 2025].

[7] M. Gohar and G. Nencioni, "The Role of 5G Technologies in a Smart City: The Case for Intelligent Transportation System," Sustainability, vol. 13, 2021. [Online]. Available: https://doi.org/10.3390/su13095188

[8] M. Attaran, "The impact of 5G on the evolution of intelligent automation and industry digitization," J. Ambient Intell. Human Comput., vol. 14, pp. 5977–5993, 2023. [Online]. Available: https://doi.org/10.1007/s12652-020-02521-x

[9] F. Cavaliere, S. Dahlfort, A. Tartaglia, J. Bergström, A. Tavemark, P. Åkerström, and D. Sinicrope, "Optimized Optical Solutions for Mobile Transport Networks," Ericsson White Paper, GFTL-22:000324 Uen, Mar. 2022. [Online]. Available: https://www.ericsson.com/494925/assets/local/reports-papers/white-papers/optimized-optical-solutions-for-mobile-transport-networks.pdf[Accessed: May 2, 2025].

[10] A. Tartaglia, "Higher Speed Optics for RAN," Nov. 2023. [Online]. Available: https://mopa-alliance.org/wp-content/uploads/2023/11/Higher-Speed-Optics-for-RAN.pdf. [Accessed: May 2, 2025].

[11] Ericsson, "Embarking the Evolution: The Future of Mobile Transport," Feb. 17, 2022. [Online]. Available: https://www.ericsson.com/491b5f/assets/local/mobile-transport/doc/17022022-embarking-the-evolution-report.pdf [Accessed: May 2, 2025].

[12] R. Hui and M. O'sullivan, "Optical Fiber Measurement," in Fiber-Optic Measurement Techniques, 2nd ed. Academic Press, 2023, ch. 4, pp. 447-555. [Online]. Available: https://doi.org/10.1016/B978-0-323-90957-0.00006-0

[13] Villafranca, Asier & Lasobras, Javier & Garcés, Ignacio. (2007). "Precise characterization of the frequency chirp in directly modulated DFB lasers." 2007 Spanish Conference on Electron Devices, Proceedings. 173 - 176. 10.1109/SCED.2007.384020.

[14] Govind P. Agrawal, "Optical Fibers," in Fiber-Optic Communication Systems, John Wiley & Sons, Ltd., 2010, pp. 24–78. Available: https://onlinelibrary.wiley.com/doi/abs/10.1002/9780470918524.ch2 DOI: 10.1002/9780470918524.ch2.

[15] F. Koyama and K. Iga, "Frequency chirping in external modulators," in Journal of Lightwave Technology, vol. 6, no. 1, pp. 87-93, Jan. 1988, doi: 10.1109/50.3969

[16] H. Zhang, S. Krooswyk, and J. Ou, "PCB design for signal integrity," in High Speed Digital Design. Morgan Kaufmann, 2015, ch. 2, pp. 27-115. [Online]. Available: https://doi.org/10.1016/B978-0-12-418663-7.00002-2

[17] Optical Internetworking Forum, "Implementation Agreement OIF-CEI-05.2: Common Electrical I/O (CEI)" Section 27.2.4.3, pp. 621-626 January 6, 2024. [Online]. Available: https://www.oiforum.com/wp-content/uploads/OIF-CEI-05.2.pdf

[18] X. Zhou and H. Liu, "Linear Pluggable Optics Beyond 112G: Where is the use case?", 2024. [Online]. Available: https://storage.googleapis.com/gweb-research2023-media/pubtools/7705.pdf

A

Appendix 1

Here we provide a more complete list of eye diagrams of different simulations with varying speed, reach, dispersion and chirp. All specific details are in the top of the image.

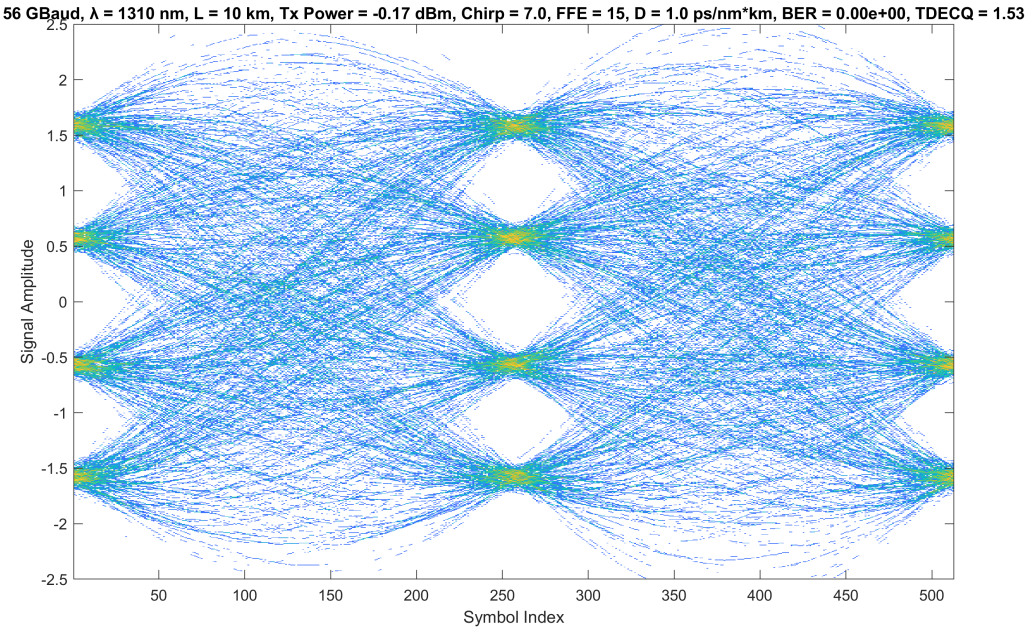

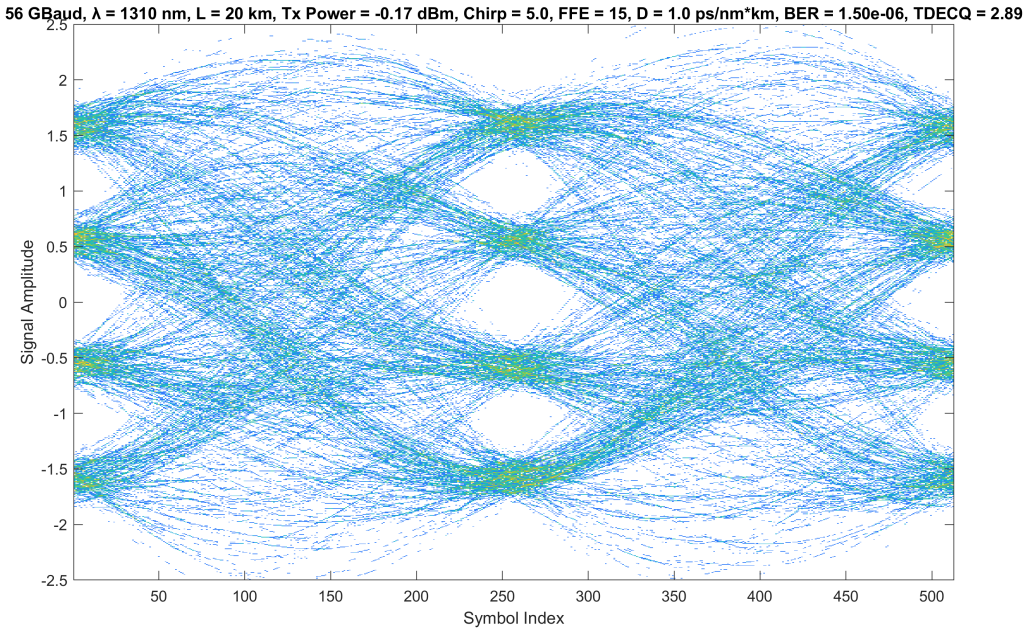
56 GBaud, λ = 1310 nm, L = 20 km, Tx Power = -0.17 dBm, Chirp = 5.0, FFE = 15, D = 1.0 ps/nm*km, BER = 1.50e-06, TDECQ = 2.89
Signal Amplitude
Symbol Index
2.5
2
1.5
1
0.5
0
-0.5
-1
-1.5
-2
-2.5
50
100
150
200
250
300
350
400
450
500

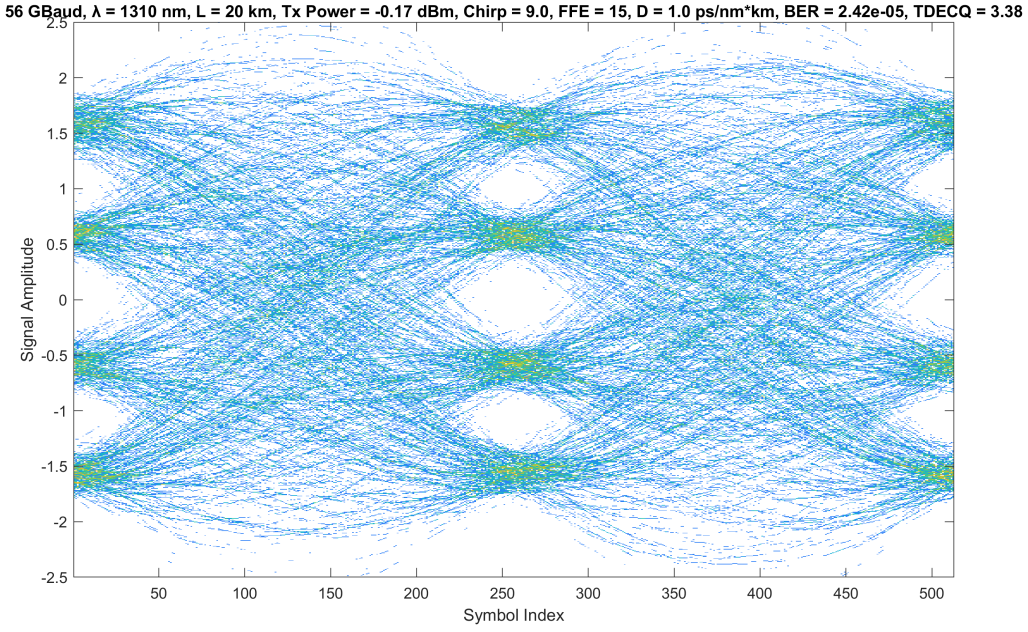
56 GBaud, λ = 1310 nm, L = 20 km, Tx Power = -0.17 dBm, Chirp = 9.0, FFE = 15, D = 1.0 ps/nm*km, BER = 2.42e-05, TDECQ = 3.38
Signal Amplitude
Symbol Index
2.5
2
1.5
1
0.5
0
-0.5
-1
-1.5
-2
-2.5
50
100
150
200
250
300
350
400
450
500

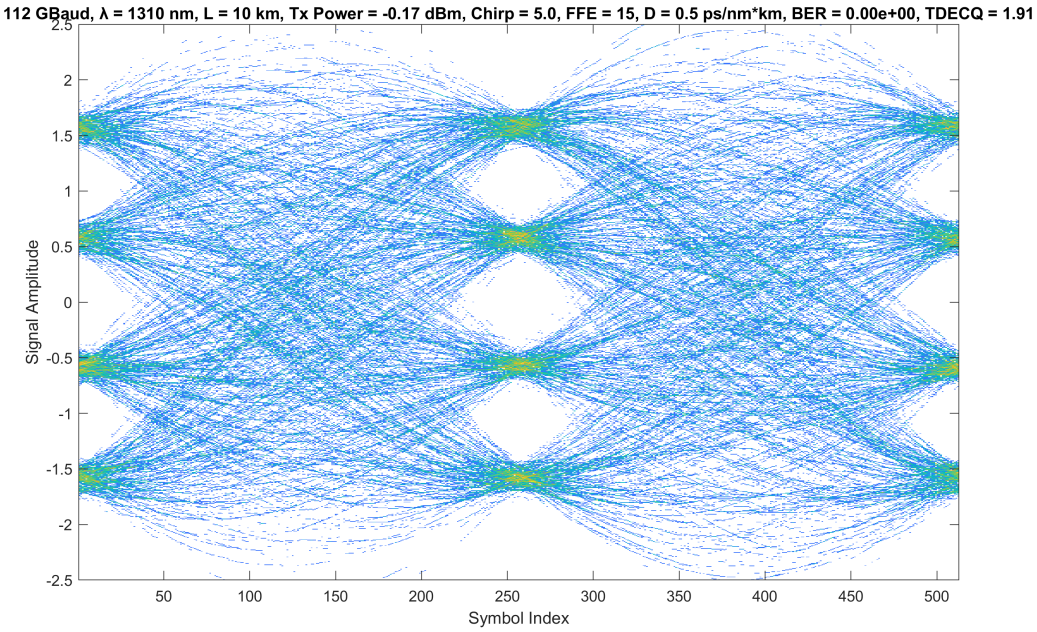
112 GBaud, λ = 1310 nm, L = 10 km, Tx Power = -0.17 dBm, Chirp = 5.0, FFE = 15, D = 0.5 ps/nm*km, BER = 0.00e+00, TDECQ = 1.91
Signal Amplitude
Symbol Index
2.5
2
1.5
1
0.5
0
-0.5
-1
-1.5
-2
-2.5
50
100
150
200
250
300
350
400
450
500

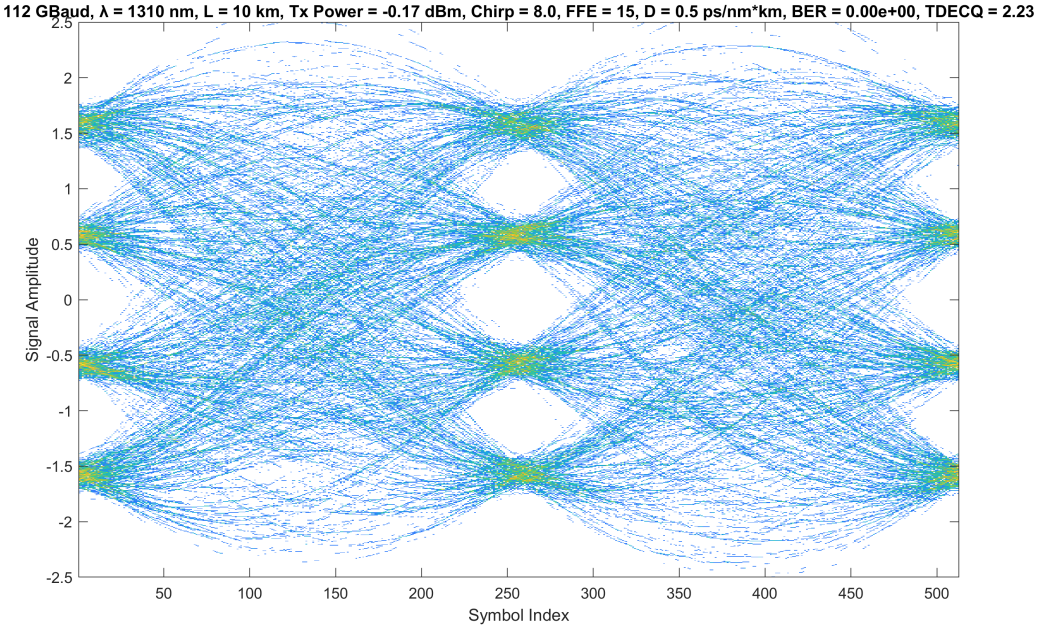
112 GBaud, λ = 1310 nm, L = 10 km, Tx Power = -0.17 dBm, Chirp = 8.0, FFE = 15, D = 0.5 ps/nm*km, BER = 0.00e+00, TDECQ = 2.23
Signal Amplitude
Symbol Index
2.5
2
1.5
1
0.5
0
-0.5
-1
-1.5
-2
-2.5
50
100
150
200
250
300
350
400
450
500

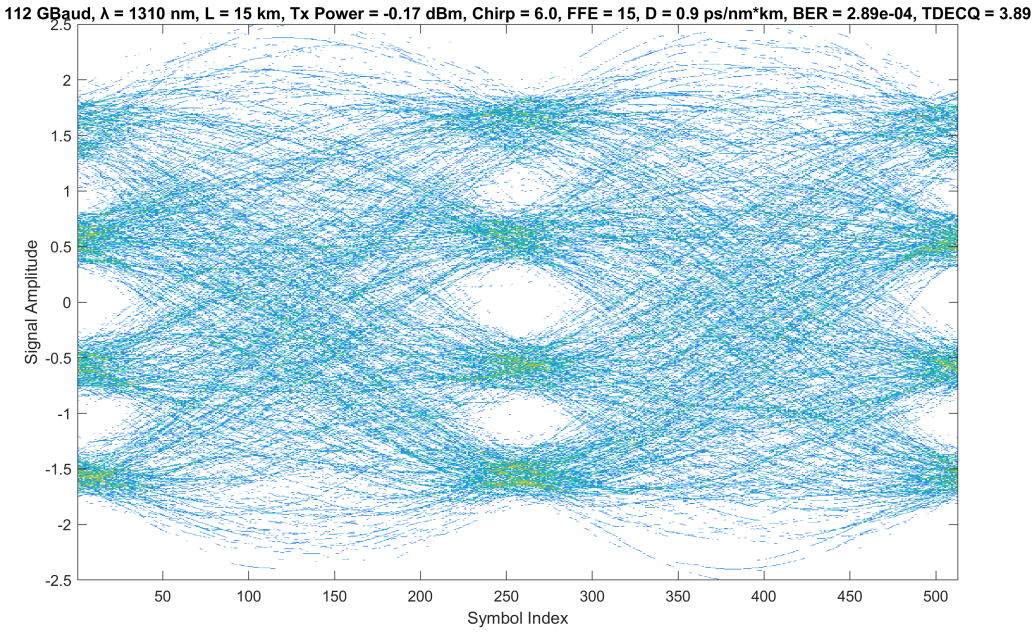
112 GBaud, λ = 1310 nm, L = 15 km, Tx Power = -0.17 dBm, Chirp = 6.0, FFE = 15, D = 0.9 ps/nm*km, BER = 2.89e-04, TDECQ = 3.89
Signal Amplitude
Symbol Index
2.5
2
1.5
1
0.5
0
-0.5
-1
-1.5
-2
-2.5
50
100
150
200
250
300
350
400
450
500

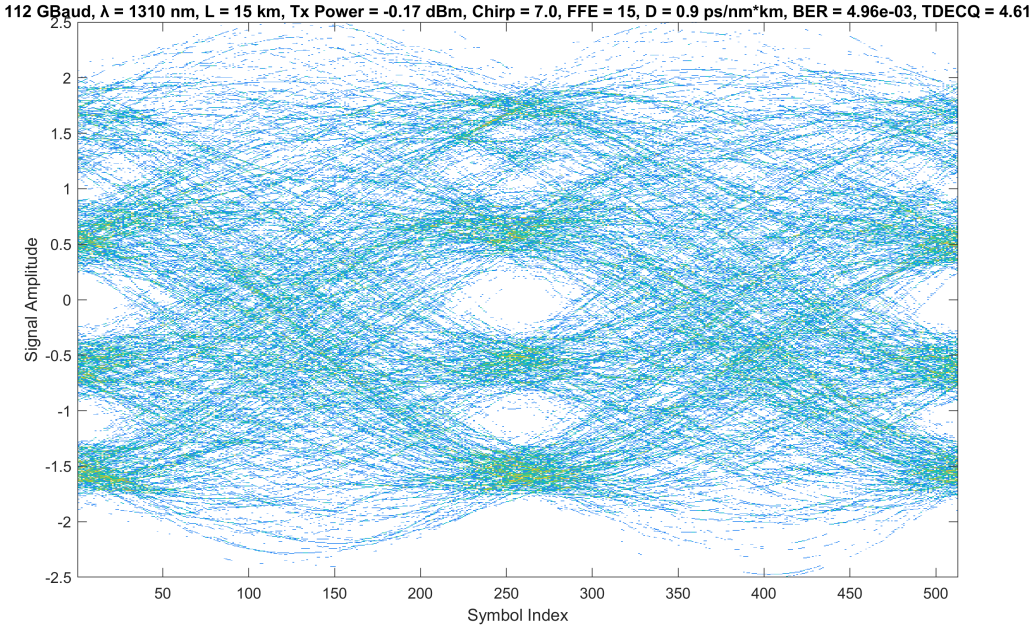
112 GBaud, λ = 1310 nm, L = 15 km, Tx Power = -0.17 dBm, Chirp = 7.0, FFE = 15, D = 0.9 ps/nm*km, BER = 4.96e-03, TDECQ = 4.61
Signal Amplitude
Symbol Index
2.5
2
1.5
1
0.5
0
-0.5
-1
-1.5
-2
-2.5
50
100
150
200
250
300
350
400
450
500

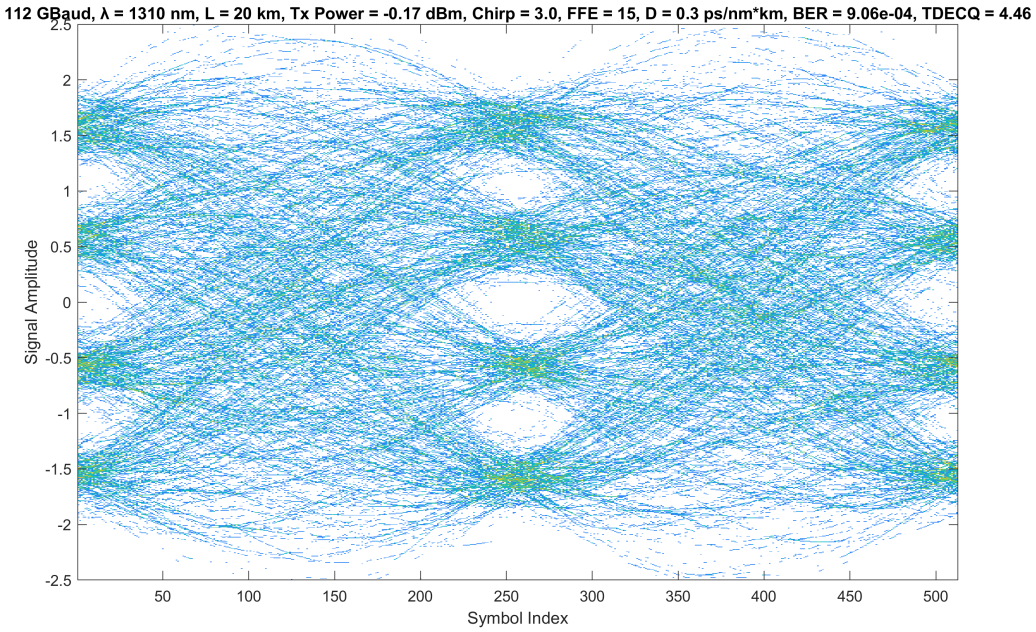
112 GBaud, λ = 1310 nm, L = 20 km, Tx Power = -0.17 dBm, Chirp = 3.0, FFE = 15, D = 0.3 ps/nm*km, BER = 9.06e-04, TDECQ = 4.46
Signal Amplitude
Symbol Index
2.5
2
1.5
1
0.5
0
-0.5
-1
-1.5
-2
-2.5
50
100
150
200
250
300
350
400
450
500

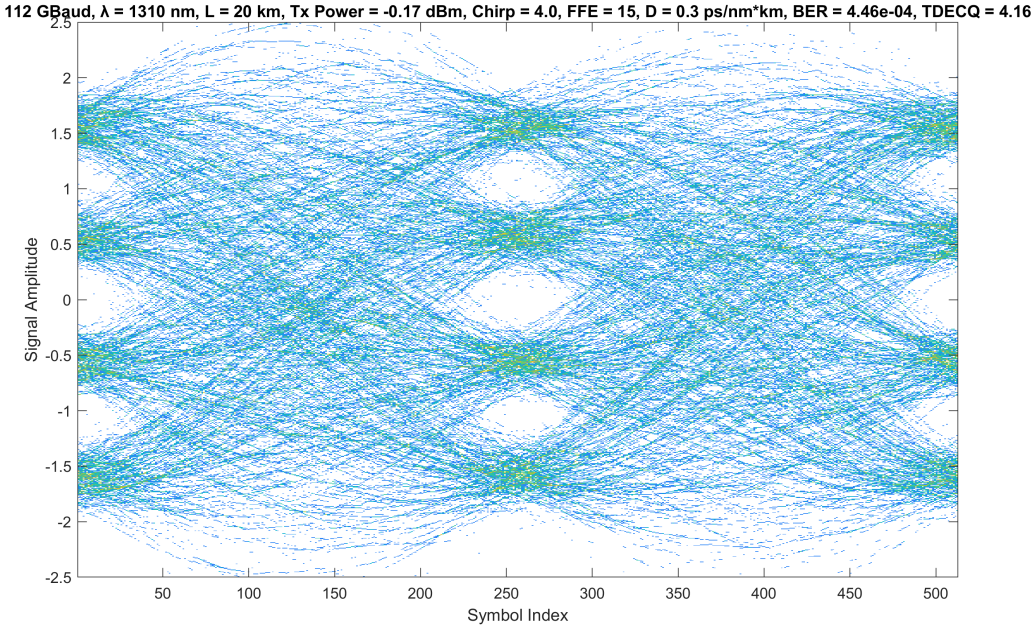
112 GBaud, λ = 1310 nm, L = 20 km, Tx Power = -0.17 dBm, Chirp = 4.0, FFE = 15, D = 0.3 ps/nm*km, BER = 4.46e-04, TDECQ = 4.16
Signal Amplitude
Symbol Index
2.5
2
1.5
1
0.5
0
-0.5
-1
-1.5
-2
-2.5
50
100
150
200
250
300
350
400
450
500

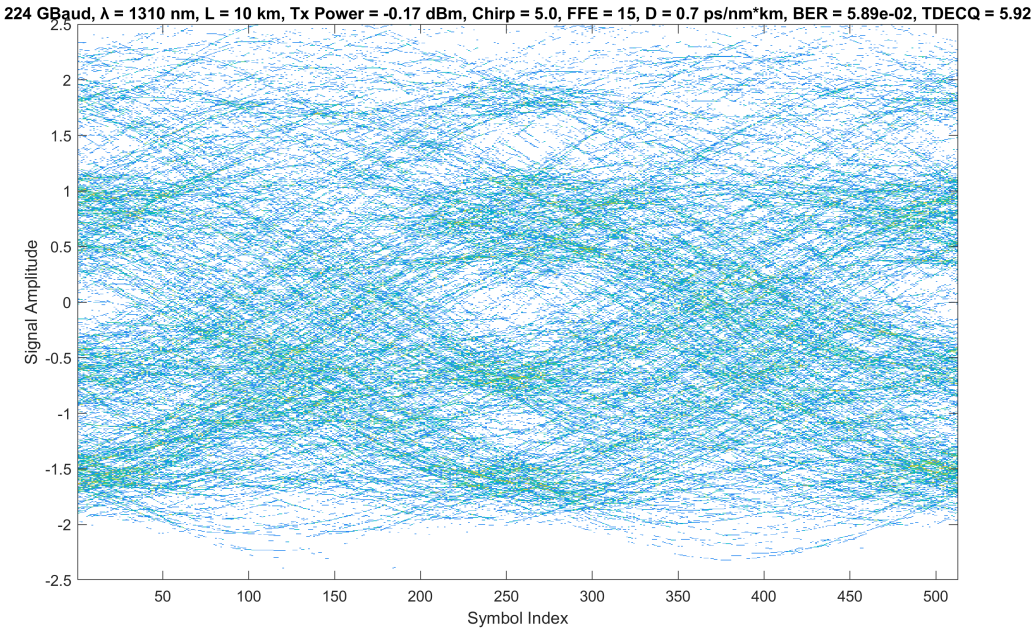
224 GBaud, λ = 1310 nm, L = 10 km, Tx Power = -0.17 dBm, Chirp = 5.0, FFE = 15, D = 0.7 ps/nm*km, BER = 5.89e-02, TDECQ = 5.92
Signal Amplitude
Symbol Index
2.5
2
1.5
1
0.5
0
-0.5
-1
-1.5
-2
-2.5
50
100
150
200
250
300
350
400
450
500

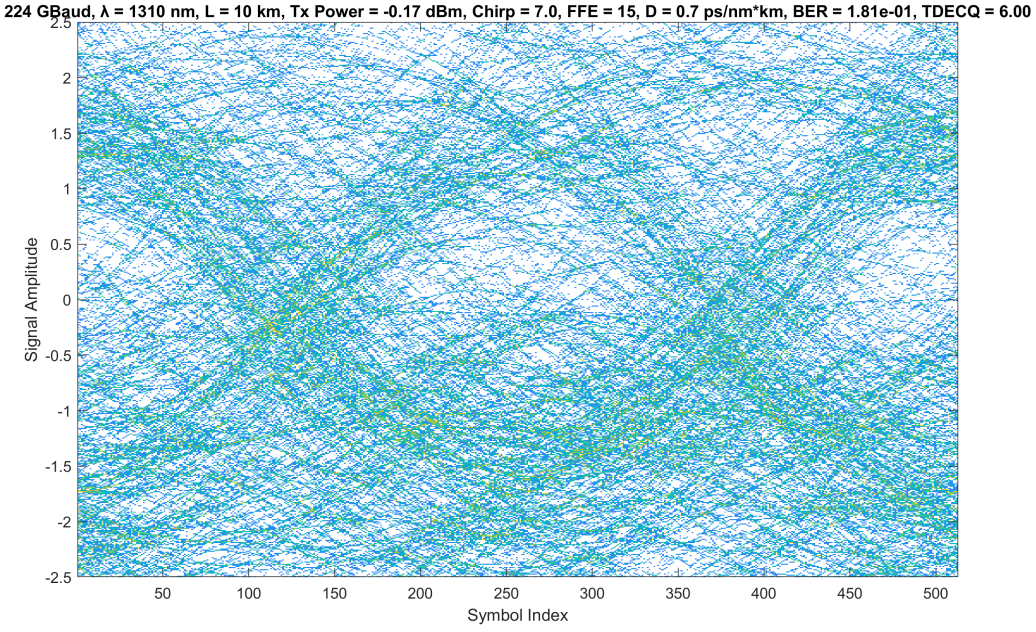
224 GBaud, λ = 1310 nm, L = 10 km, Tx Power = -0.17 dBm, Chirp = 7.0, FFE = 15, D = 0.7 ps/nm*km, BER = 1.81e-01, TDECQ = 6.00
Signal Amplitude
Symbol Index
2.5
2
1.5
1
0.5
0
-0.5
-1
-1.5
-2
-2.5
50
100
150
200
250
300
350
400
450
500

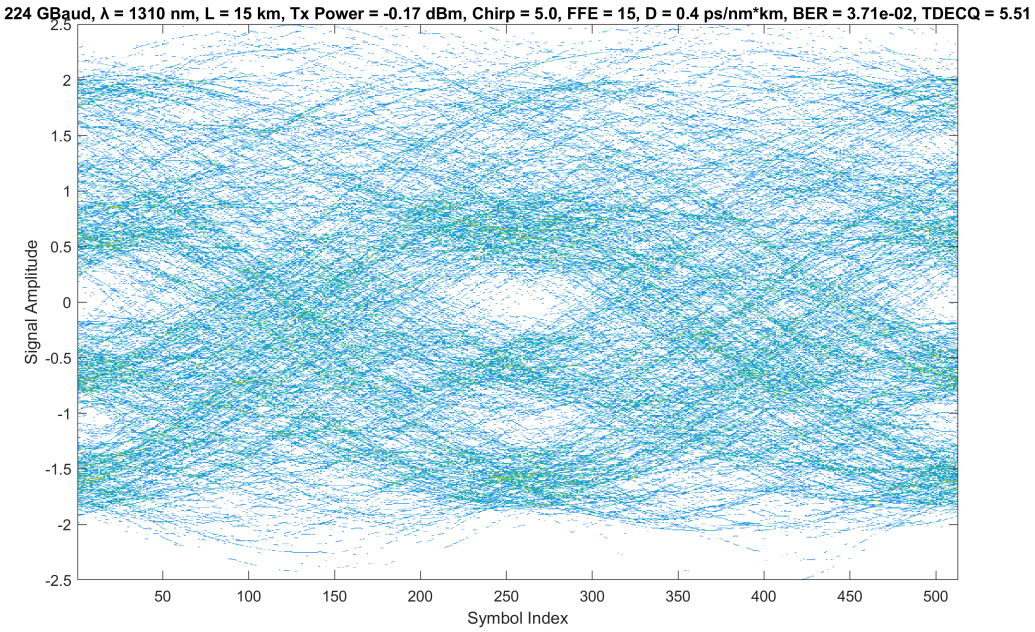
224 GBaud, λ = 1310 nm, L = 15 km, Tx Power = -0.17 dBm, Chirp = 5.0, FFE = 15, D = 0.4 ps/nm*km, BER = 3.71e-02, TDECQ = 5.51
Signal Amplitude
Symbol Index
2.5
2
1.5
1
0.5
0
-0.5
-1
-1.5
-2
-2.5
50
100
150
200
250
300
350
400
450
500

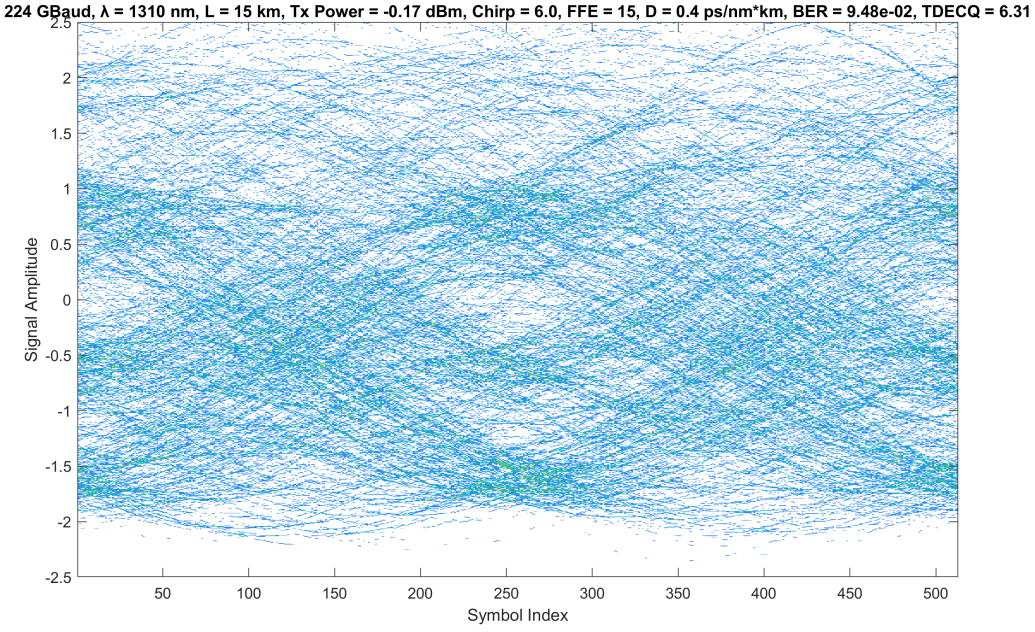
224 GBaud, λ = 1310 nm, L = 15 km, Tx Power = -0.17 dBm, Chirp = 6.0, FFE = 15, D = 0.4 ps/nm*km, BER = 9.48e-02, TDECQ = 6.31
Signal Amplitude
Symbol Index
2.5
2
1.5
1
0.5
0
-0.5
-1
-1.5
-2
-2.5
50
100
150
200
250
300
350
400
450
500

DEPARTMENT OF ELECTRICAL ENGINEERING
CHALMERS UNIVERSITY OF TECHNOLOGY
Gothenburg, Sweden
www.chalmers.se

CHALMERS
UNIVERSITY OF TECHNOLOGY